AGU PUBLICATIONS

Water Resources Research

RESEARCH ARTICLE
10.1002/2017WR021289

Key Points:
- Exposure time distributions quantified using hydrodynamic modeling are affected by the hydrological connectivity between channels and islands
- Transport within deltaic islands comprises a significant fraction of the network exposure time distribution
- Deltaic islands have relatively long exposure times compared to delta channels, which makes them hot spots for nitrate removal

Supporting Information:
- Supporting Information S1

Correspondence to:
P. Passalacqua,
paola@austin.utexas.edu

Citation:
Hiatt, M., Castañeda-Moya, E., Twilley, R., Hodges, B. R., & Passalacqua, P. (2018). Channel-island connectivity affects water exposure time distributions in a coastal river delta. *Water Resources Research*, *54*, 2212–2232. https://doi.org/10.1002/2017WR021289

Received 15 JUN 2017
Accepted 1 MAR 2018
Accepted article online 6 MAR 2018
Published online 25 MAR 2018

Channel-Island Connectivity Affects Water Exposure Time Distributions in a Coastal River Delta

Matthew Hiatt[1,2], Edward Castañeda-Moya[2,3], Robert Twilley[2], Ben R. Hodges[1], and Paola Passalacqua[1]

[1]Department of Civil, Architectural, and Environmental Engineering, Center for Water and the Environment, University of Texas at Austin, Austin, TX, USA, [2]Department of Oceanography and Coastal Sciences, Louisiana State University, Baton Rouge, LA, USA, [3]Now at Southeast Environmental Research Center, Florida International University, Miami, FL, USA

Abstract The exposure time is a water transport time scale defined as the cumulative amount of time a water parcel spends in the domain of interest regardless of the number of excursions from the domain. Transport time scales are often used to characterize the nutrient removal potential of aquatic systems, but exposure time distribution estimates are scarce for deltaic systems. Here we analyze the controls on exposure time distributions using a hydrodynamic model in two domains: the Wax Lake delta in Louisiana, USA, and an idealized channel-island complex. In particular, we study the effects of river discharge, vegetation, network geometry, and tides and use a simple model for the fractional removal of nitrate. In both domains, we find that channel-island hydrological connectivity significantly affects exposure time distributions and nitrate removal. The relative contributions of the island and channel portions of the delta to the overall exposure time distribution are controlled by island vegetation roughness and network geometry. Tides have a limited effect on the system's exposure time distribution but can introduce significant spatial variability in local exposure times. The median exposure time for the WLD model is 10 h under the conditions tested and water transport within the islands contributes to 37–50% of the network-scale exposure time distribution and 52–73% of the modeled nitrate removal, indicating that islands may account for the majority of nitrate removal in river deltas.

Plain Language Summary The transport of nutrients to coastal waters can cause a number of environmental, economic, and human health issues. For example, the Gulf of Mexico's "Dead Zone" off the coast of Louisiana is one of the largest hypoxic (low oxygen) zones in the world and its increasing size has been attributed to increased nutrient delivery by the Mississippi River. There is evidence that river deltas may be able to naturally reduce the nutrient load to coastal waters by removing nutrients. One important factor for predicting nutrient removal in a coastal system is the water transport time scale, or how long water stays in the system. In systems like river deltas, which comprise a complex network of channels and inundated islands that behave as vegetated wetlands, the water transport time scale can vary significantly in time and space. Our research aims to identify how vegetation, river discharge, tides, and channel network geometry influence the water transport time scale in a coastal river delta. We highlight how the transport of water from the channels to the deltaic wetlands influences the water transport time scale. Our work is relevant to planned engineered river diversions in the Mississippi River Delta, which will alter water transport time scales in the region.

1. Introduction

Water transport time scales give an indication of the retention time of material suspended in the water column (e.g., dissolved nutrients). Such time scales are often compared to biogeochemical processing time scales to estimate nutrient removal. Among the many transport time scales, the water residence time, generally defined as the time required for a water parcel to exit a domain (Monsen et al., 2002; Zimmerman, 1976), has been studied extensively in estuaries (Brooks et al., 1999; Camacho & Martin, 2013; de Brye et al., 2012; Perez et al., 2011; Shen & Haas, 2004; Wang et al., 2004; Yuan et al., 2007), lagoons (Cucco & Umgiesser, 2006; Umgiesser et al., 2014), and wetlands (Musner et al., 2014; Werner & Kadlec, 2000; Wörman

& Kronnäs, 2005). However, in systems subject to flow direction reversal across the boundary (e.g., due to a flood tide), the total time a water parcel spends in the domain can be underestimated by the residence time (Monsen et al., 2002), leading to the adoption of the exposure time, or the cumulative amount of time a water parcel spends in the control volume regardless of its excursions outside the domain (e.g., de Brauwere et al., 2011; de Brye et al., 2012; Delhez, 2013; Monsen et al., 2002; Viero & Defina, 2016). Despite the environmental importance of river deltas, the study of water transport time scales in coastal river deltas is relatively nascent (Hiatt & Passalacqua, 2015; Sawyer et al., 2015; Sendrowski & Passalacqua, 2017). The goal of this paper is to quantify controls on the exposure time distribution (ETD) in a coastal river delta.

The transport of water in river deltas is not limited to the channel network as these systems are characterized by hydrological connectivity (HC) between channels and inundated islands, adding complexity to the analysis of water-mediated transport of sediment and solutes (Passalacqua, 2017). HC is defined as the transport of water, sediment, and nutrients among various components of a landscape (Bracken et al., 2013; Tetzlaff et al., 2007). Field work at Wax Lake delta (WLD) in coastal Louisiana, USA, showed that 23–54% of the water flux entering WLD is allocated to the deltaic islands (Hiatt & Passalacqua, 2015), which are partially vegetated freshwater marshes that are flanked by subaerial levees. Numerical modeling efforts (Hiatt & Passalacqua, 2017) and an independent analysis of delta bathymetry (Shaw et al., 2016a) have shown similar results. Using a dye tracer within an island and acoustic Doppler current profiler measurements in channels at WLD, Hiatt and Passalacqua (2015) showed that transport times in the islands are significantly longer than in the channels, suggesting that ETDs are likely strongly dependent on the HC between channels and islands. Given that WLD is often considered a prototype system for land-building and nutrient removal efforts through river diversions in coastal Louisiana (Allison & Meselhe, 2010; Henry & Twilley, 2014; Kim et al., 2009; Paola et al., 2011), understanding the controls on ETDs in this system is relevant to restoration efforts.

River discharge, tides, and the system geometry all affect water transport in coastal deltas. The increased hydraulic resistance associated with flow through vegetation (Kadlec, 1990; Nepf, 1999; Nepf & Vivoni, 2000) also likely impacts transport times (Nepf et al., 2007), as well as the allocation of flow between channels and vegetated portions of the system (Musner et al., 2014). Sediment grain size affects the surface water-groundwater connectivity and groundwater residence time distributions in deltas (Sawyer et al., 2015), but the controls on surface water transport time scales, which are commonly used for estimating nutrient removal in wetland and estuarine systems (e.g., Cheng & Basu, 2017; Dettmann, 2001; Nixon et al., 1996; Yu et al., 2006), have yet to be quantified.

System-scale physical transport time scales are essential for obtaining nutrient removal estimates at large scales (Rivera-Monroy et al., 2010). Coastal wetlands, river deltas, and estuaries can mitigate increased nutrient pollution delivered to receiving waters (Diaz & Rosenberg, 2008) by acting as nutrient sinks (DeLaune et al., 2005; Dettmann, 2001; Lane et al., 2003; Luu et al., 2012; Mitsch et al., 2001; Perez et al., 2011; Yu et al., 2006). To the first order, nutrient removal efficiency depends on the relative time scales of physical transport and biogeochemical processes. Using direct measurements of denitrification and a denitrification model, Yu et al. (2006) showed that nitrate removal efficiencies ranged from $42 \pm 2.5\%$ to $95 \pm 0.5\%$ depending on water residence time at the Davis Pond Freshwater Diversion Project (Louisiana, USA). Yearly fractional nitrate removal in estuaries has been modeled as a function of freshwater residence time and a first-order decay rate (Dettmann, 2001), and the simple model was found to adequately represent field data. The link between transport times and nutrient removal generally relies on a single representative value for transport time scale (e.g., Cheng & Basu, 2017; Dettmann, 2001; Nixon et al., 1996; Perez et al., 2011; Yu et al., 2006). However, due to variability in flow paths and environmental conditions in natural systems, a statistical description of the transport times in terms of a probability distribution is more representative (Kadlec, 2012; Musner et al., 2014; Somes et al., 1999).

Improved predictions of the ecological and water quality impacts of proposed river diversions should be facilitated by improved understanding of the physical controls on river delta ETD. This paper seeks to identify the processes controlling ETD in a branching river delta network using an idealized setting and the WLD bathymetry as the test beds. We analyze the effects of river discharge, tidal amplitude, hydraulic roughness due to vegetative drag, and network structure on ETD using a hydrodynamic model. Additionally, following the work of Dettmann (2001), we apply a simple nitrate removal model to our ETD results to quantify spatial

variability in nitrate removal and to highlight the relative contributions of deltaic channels and islands to nutrient removal.

This paper is organized as follows. We first introduce a two-dimensional hydrodynamic and scalar transport model, followed by a summary of the model boundary conditions and the calculations of ETD and nitrate removal (section 2). Then we present results showing the effects of river discharge, tides, network geometry, and hydraulic roughness on ETD and nitrate removal (section 3). A discussion of the results and implications for the restoration of coastal wetlands follows, along with a qualitative comparison of the model results to field measurements of nitrate concentrations at WLD (section 4). Finally, we state our conclusions (section 5).

2. Methods

2.1. Hydrodynamic Model Description

We model the hydrodynamics in two horizontal dimensions with the Fine Resolution Environmental Hydrodynamics model (Frehd). The model solves the shallow water equations using the computational schemes of Casulli and Cheng (1992), Casulli and Cattani (1994), Hodges et al. (2000), Stelling and Zijlema (2003), Hodges (2004, 2014), and Hodges and Rueda (2008). The modeling setup in the present study is similar to the modeling work of Hiatt and Passalacqua (2017), who used Frehd to characterize the transition from confined to unconfined flow at WLD.

2.2. Hydrodynamic Model Governing Equations

Frehd implements the depth-integrated solution of the hydrostatic Navier-Stokes equations with the Boussinesq approximation (i.e., shallow water equations), written as

$$\frac{\partial u_i}{\partial t}+u_j\frac{\partial u_i}{\partial x_j}+g\frac{\partial \eta}{\partial x_i}-v_e\frac{\partial^2 u_i}{\partial x_j \partial x_j}+\frac{C_R|V|}{2H}u_i=0 \quad : \quad i=\{1,2\} \tag{1}$$

$$\frac{\partial \eta}{\partial t}+\frac{\partial}{\partial x_j}Hu_j=0 \tag{2}$$

where a modified Einstein convention is used for summation over $j=\{1,2\}$ for repeated subscripts, u_i are the depth-averaged horizontal velocities in the x_i directions (m s^{-1}), $|V|=\left(u_1^2+u_2^2\right)^{1/2}$ is the horizontal velocity magnitude (m s^{-1}), g is the gravitational acceleration (m s^{-2}), v_e is a horizontal eddy viscosity (m^2 s^{-1}), C_R is the bottom drag coefficient, H is the local depth (m), η is the free surface elevation (m), and t is time (s). The horizontal eddy viscosity v_e (Cea et al., 2007) is set to 0.01 m^2 s^{-1} (Hiatt & Passalacqua, 2017) based on the depth-averaged equation for shear velocity of Wilcock (1996), typical flow characteristics at WLD (Hiatt & Passalacqua, 2015), and grain size values (Shaw & Mohrig, 2014) measured at WLD (supporting information).

2.3. Tracer Propagation

The transport of a passive tracer in Frehd is modeled with the conservative advection/diffusion equation (Hodges, 2014),

$$\frac{\partial cH}{\partial t}+\frac{\partial}{\partial x_j}u_j cH-\kappa_e\frac{\partial}{\partial x_j}\left(H\frac{\partial c}{\partial x_j}\right)=0 \tag{3}$$

where c is the depth-averaged tracer concentration (kg m^{-3}) and κ_e is the eddy diffusivity (m^2 s^{-1}). To ensure the tracer passively traces the flow field, κ_e is set to the same magnitude as v_e (0.01 m^2 s^{-1}).

A particle tracking code is used to quantify ETDs at every model grid cell over multiple modeling scenarios. We modify the stochastic particle tracking code of DeltaRCM (Liang et al., 2015, 2016) to handle temporally variable velocity fields. The velocity field is used to advect particles at each time step and an isotropic random walk technique is used to model diffusive processes as

$$x_{i,t+\Delta t}=x_{i,t}+(u_{i,t}+D\Phi)\Delta t \tag{4}$$

where $x_{i,t+\Delta t}$ is the new location of the particle at time $t+\Delta t$, $u_{i,t}$ is the component of velocity in the i direction at time t, D is a calibrated diffusion velocity set to 0.20 m s^{-1}, and Φ is a random number between -0.5 and 0.5 that ensures isotropic diffusion (Liang et al., 2016). The method is equivalent to other

Lagrangian particle tracking codes utilized in studies of water transport time scales in coastal environments (e.g., Meyers & Luther, 2008). The values selected for D and Φ ensure that the diffusive component of particle transport is relatively small compared to the advective component. The diffusion velocity is parameterized to produce mass flux distributions (section 2.6) at the system boundary that match those calculated with equation (3) for the steady state case (supporting information). A Wilcoxon rank-sum test at the 5% significance level shows that the particle tracking and the advection/diffusion tracer methods produce equivalent mass flux distributions for all relevant scenarios (supporting information).

2.4. Model Domains and Boundary Conditions

The WLD is a naturally prograding river delta located about 140 km southwest of New Orleans in coastal Louisiana (Figure 1a). The delta has been building land since 1973 and is currently prograding at a rate greater than 200 m yr^{-1} (Shaw et al., 2013). The median discharge is about 3,000 m^3 s^{-1} (USGS, 2016) and the average tidal range in the region is about 0.35 m (NOAA, 2016), although the tidal range can approach nearly 1 m during spring tides. WLD comprises a network of distributary channels and inundated interdistributary deposits flanked by subaerially exposed levees; these zones are commonly referred to as deltaic islands (e.g., Edmonds et al., 2011; Fagherazzi et al., 2015; Passalacqua, 2017). The WLD islands are freshwater wetlands (Howes et al., 2010) populated by vegetation species that exhibit zonation along the elevation gradient (Bevington et al., 2017; Carle et al., 2013). The WLD islands show significant connectivity with the distributary channels and up to 54% of the distributary channel discharge is delivered to the islands before reaching the delta front (Hiatt & Passalacqua, 2015, 2017; Shaw et al., 2016a). Saline intrusion in the region is limited to storm events (Holm & Sasser, 2001; Walker, 2001).

Two modeling domains are used: a simplified schematic channel-island complex (CIC) representative of typical geometries from a channel-island complex at WLD following the conceptual model of Hiatt and Passalacqua (2015) (Figure 1d) and the topography/bathymetry of WLD (Figure 1e; Shaw et al., 2016b). Both domains are nested within a larger buffer domain to eliminate any spurious boundary reflections and properly account for backwater effects. Each domain utilizes a regular square grid with a cell size of 50 m and a constant time step of 25 s is used for all runs (Table 1). The geometries and construction of the computational domains are described thoroughly in Hiatt and Passalacqua (2017). This study quantifies ETDs for the hydrodynamic model runs presented in Hiatt and Passalacqua (2017) and for additional model runs that account for the influence of tides.

The CIC model is used to represent the typical geometry of a distributary channel at WLD flanked by two islands. The domain represents a fundamental unit of a more complicated delta network and can be used for hypothesis testing on deltaic hydraulics without the additional complexity introduced by a complete network flow field (Hiatt & Passalacqua, 2017; Shaw et al., 2016a). We test two constant river discharges of 300 and 700 m^3 s^{-1} based on discharge measurements taken during average flow conditions in two representative WLD channels with geometries similar to that of the CIC (Hiatt & Passalacqua, 2017), while the seaward water level is maintained at a constant $\eta = 0$ m in both cases. A numerical tracer (equation (3)) is released in the channel portion ($x_1 = 107.5$ km) of the CIC and is allowed to propagate through the domain. The ETD is calculated at the downstream boundary x_b (equation (10)) and is separated into the contributions of the channel and the islands (e_1 and e_2, respectively). The influence of vegetative drag (see following section) within the delta islands on ETD is also tested.

The WLD model is used to test the influences of tidal water level fluctuations and spatial patterns in the topography on ETD. Our aim with the WLD model is to test the influences of tides and structure of the delta network on ETD in an uncalibrated setting, rather than to make high-fidelity predictions of ETD with a complex model. Thus, our study aims to enhance our understanding of the processes controlling ETD in a branching deltaic network using WLD as our test site. We subjected the WLD model to a constant river discharge of $Q_R = 3{,}300$ m^3 s^{-1} at the landward boundary and forced the model with a spring-neap tidal cycle at the seaward boundary. The discharge was chosen as a representative value based on discharge measurements entering WLD on 20 June 2015 (supporting information). The tidal boundary condition was generated as

$$\eta(t) = \sum_{n=1}^{N} A_n \cos(\sigma_n t - G_n) \tag{5}$$

where A_n is the tidal amplitude (m), σ_n is the angular speed (rad h^{-1}), G_n is the phase lag (rad), t is time (h), and N is the number of tidal constituents. The S2 (principal solar semidiurnal) and M2 (principal lunar

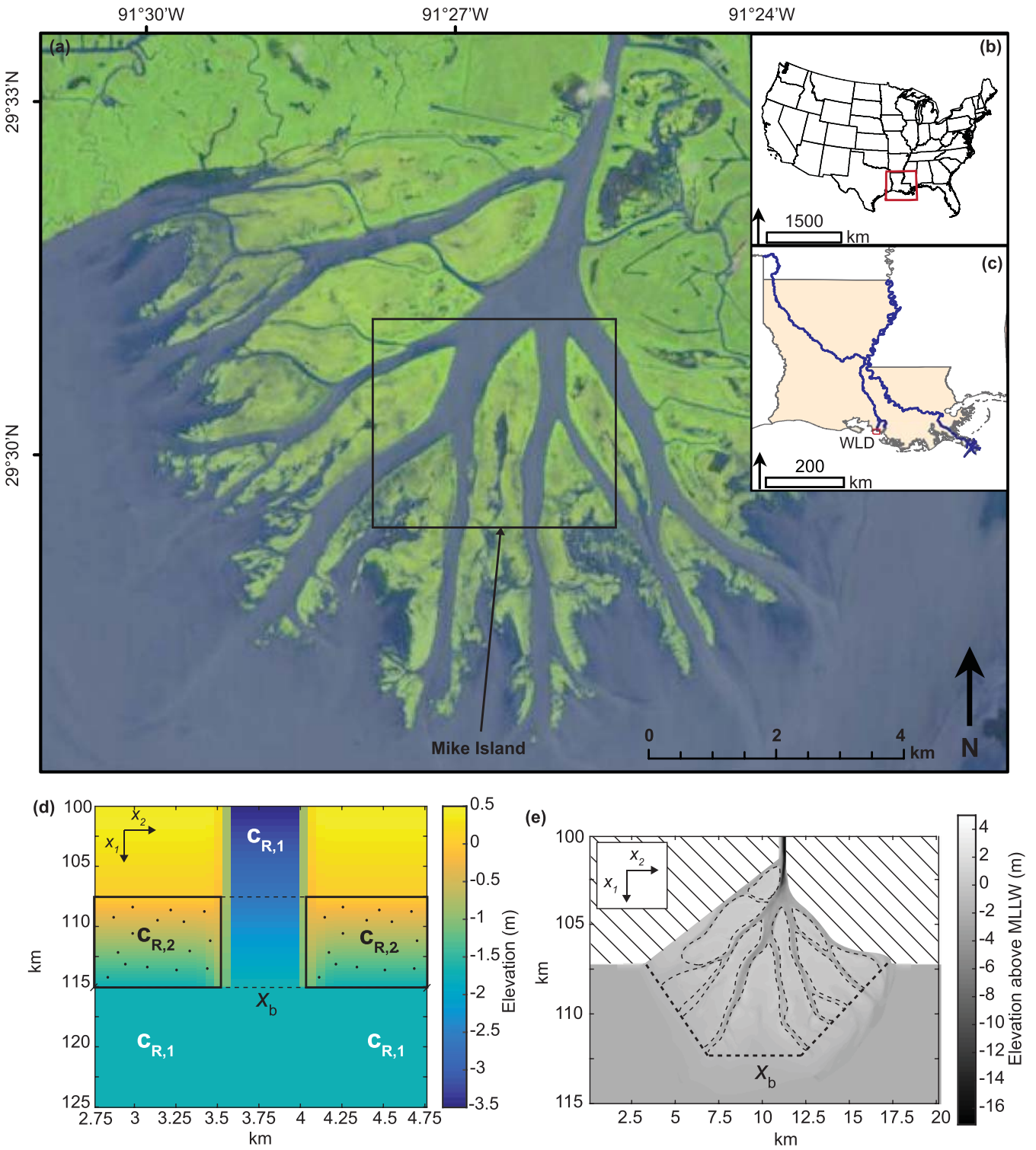

Figure 1. Study site and modeling domains (after Hiatt & Passalacqua, 2017). (a) Map of the Wax Lake delta (WLD) in coastal Louisiana, USA. The satellite image is from Landsat TM 5 taken on 19 June 2014 (accessible at http://glovis.usgs.gov). (b) Map of the USA showing the location Louisiana. (c) Map of the major river systems in Louisiana and WLD. (d) The test domain for the idealized channel-island complex parametrized by typical bathymetry and topography at WLD. (e) The test domain for the WLD model based on the bathymetric DEM generated by Shaw et al. (2016b). The test domains are nested within a larger buffer domains to alleviate spurious boundary effects (see text for details). Note that Figures 1d and 1e have different scales. The boundaries (x_b) for the calculation of ETD are delineated with dashed lines.

semidiurnal) tidal constituents from the NOAA Lawma-Amerada Pass Station (located ~8 km east of WLD) are used ($A_{S2} = 0.10$ m and $A_{M2} = 0.29$ m; NOAA, 2016). The result of equation (5) is a semidiurnal tide with a spring-neap cycle. The WLD setup has been shown to reproduce measured channel-island HC (Hiatt & Passalacqua, 2017) and the network-scale hydrodynamics have been tested against hydrographic surveys performed at WLD (supporting information).

We calculate ETDs for each location in the WLD model for a number of different modeling scenarios. First, a model run without tides is performed as a baseline scenario. We then test the influence of the spring-neap tidal cycle and the semidiurnal fluctuations on ETD. We release tracer particles at high, low, rising, and falling tides as measured at the downstream boundary of the WLD test domain and compare the resulting ETDs. This procedure is performed during both spring and neap tide.

2.5. Drag Coefficient

Water flow through vegetation is often modeled with an increased drag coefficient due to contributions from both the bed and vegetation (Kadlec, 1990; Musner et al., 2014; Nepf, 1999; Nepf & Vivoni, 2000). We model this change in the drag coefficient as

$$C_R = \frac{1}{2} C_D n h_v + C_B \tag{6}$$

where C_D is the coefficient of drag for a vertical cylinder, n is the vegetation front area per unit volume (m^{-1}), h_v is the submerged stem height (m), and C_B is the bottom drag coefficient (Baptist et al., 2007; Nardin et al., 2016). For all model runs C_B is set equal to 0.005, which is a typical value for delta systems (e.g., Nardin et al., 2016).

The CIC model is used to test the influence of vegetation roughness on ETD. We express the ratio of modified drag coefficients in the island and channel as

$$\theta = \frac{C_{R,2}}{C_{R,1}} \tag{7}$$

where the subscripts 1 and 2 represent the channel and the island zones (Figure 1d), respectively. We assume there is no vegetation within the channel portion and set $C_{R,1} = C_B$ for all model runs. A uniform value of $C_{R,2}$ is assigned to the island portions of the domain. The tested values for the modified drag within the islands are $C_{R,2} \in = \{0.001, 0.0025, 0.005, 0.01, 0.025, 0.05, 0.5\}$ corresponding to $\theta \in = \{0.2, 0.5, 1, 2, 5, 10, 100\}$. The set of $C_{R,2}$ values corresponds to $C_D a h_v \leq 1$, representing a range from sparse to dense vegetation (Lightbody & Nepf, 2006; Luhar et al., 2008; Nepf, 2012).

We test the influence of vegetation in the CIC and not in the WLD in order to isolate the effects of increased roughness on the ETD in a simplified geometry. The effect of vegetation within the deltaic islands is therefore not modeled in the WLD (i.e., $\theta = 1$ for each grid cell).

2.6. Exposure Time Distributions

Coastal river deltas may be subject to flow reversals and the typical fanlike shape of many deltas can lead to a relatively long seaward boundary as compared to semienclosed basins. Thus, river deltas may be particularly prone to oscillating or meandering flows at the seaward boundary (Figure 2), which are best handled by the exposure time (Delhez, 2013; Monsen et al., 2002). To calculate the ETD, we monitor the mass flux at the system boundary for a diffuse tracer (equation (3)) in model runs without tides (steady state). Since model runs with tides are subject to return flows across the boundary, we elect to use a particle tracking scheme (equation (4)) to quantify ETD by counting the cumulative time spent by each particle in the domain.

We provide a basic description of our method for calculating ETDs at steady state, but a full derivation is found in the supporting information. The differential travel time distribution for a pulse injection of tracer at $t = 0$ calculated at the domain boundary at time t is given as (e.g., Benjamin & Lawler, 2013):

$$E(t) = \frac{dN(t)/dt}{N_{total}} \tag{8}$$

where $dN(t)/dt$ is the rate at which material exits the domain at time t and N_{total} is the amount of material injected into the system at $t = 0$. Integrating over time gives the cumulative travel time distribution:

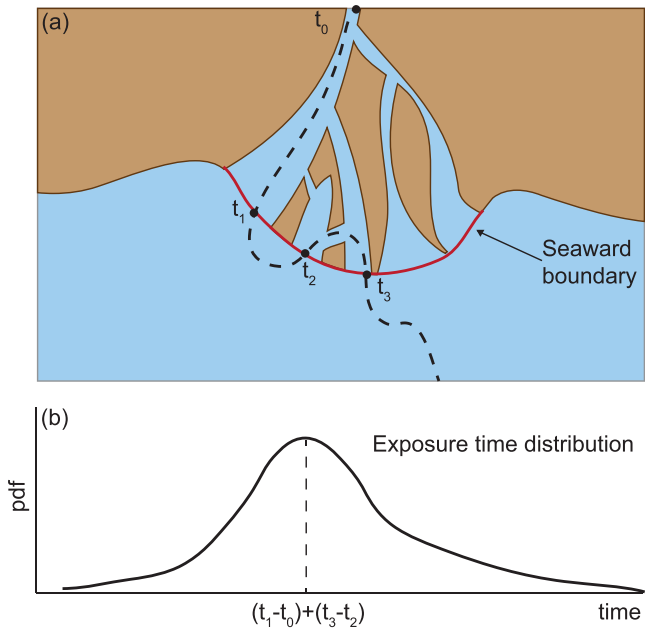

Figure 2. Conceptual representation a water parcel being transported through a river delta and a conceptual exposure time distribution. (a) A typical path for a parcel traveling through the domain (dashed line). The parcel passes through the seaward boundary at times t_1, t_2, and t_3 (after Delhez, 2013). (b) Conceptualization of the exposure time distribution. The median exposure time would typically be $(t_1-t_0)+(t_3-t_2)$.

$$F(t)=\int_0^t E(\tau)d\tau \tag{9}$$

where τ is a dummy variable and $F(t=\infty)=1$, rendering $E(t)$ and $F(t)$ the probability density function (pdf) and cumulative distribution function (cdf) of the travel time, respectively.

In a discrete steady state case, we solve for the local mass flux of tracer along the exit boundary. We then integrate spatially over the domain boundary and substitute into equation (8) to calculate differential travel time distribution:

$$E(t)=\frac{\int_{x_{b,0}}^{x_{b,n}} q_\perp(x_B,t)\cdot c(x_B,t)\,dx_B}{\int_0^\infty \int_{x_b,0}^{x_{b,n}} q_\perp(x_B,\tau)\cdot c(x_B,\tau)\,dx_B\,d\tau} \tag{10}$$

where $q_\perp$ is volumetric flowrate of water per unit length, c is the concentration of tracer (kg m^{-3}), x_B is the system boundary coordinate, and H is the water depth (m). The fractional mass flux $e_i(t)$ associated with a given region i of the domain can also be calculated in a similar fashion (supporting information). Equation (10) is solved discretely at the domain boundary at each time step for model runs without return flows and represents the system-wide ETD.

In systems subject to return flows of tracer material across the seaward boundary, the above framework is invalid, since tracer material can be accounted for in the mass flux more than once. Therefore, we utilize a lagrangian approach in these situations. The domain is seeded with particle tracers and their individual propagation is tracked; each particle is advected by the velocity field and the random walk technique (equation (4)). We count the time each particle spends in the domain of interest, regardless of the number of excursions or time spent outside the domain. The ETD for each location ($E(x_1,x_2,t)$) within the domain can then be computed. The initial concentration of the particles in each cell is determined by the local depth (or water volume) of the cell at the time of release, ensuring that the same concentration of particles is released in each cell. This lagragian approach to generating the ETD is equivalent to approaches used in other studies of water transport time scales in coastal systems (e.g., Cucco et al., 2009; Cucco & Umgiesser, 2015; Meyers & Luther, 2008).

2.7. Nitrate Removal Model

The hydrodynamic model output is coupled with a simple model for nitrate removal as a function of the ETD. We use this simple model to identify spatial heterogeneity in nitrate removal and the relative contributions of islands and channels to nitrate removal WLD. We base our model off of the fractional nitrate removal model of Dettmann (2001), which was originally developed to quantify nitrate removal via denitrification on an annual scale using freshwater residence time for estuaries (Dettmann, 2001). We quantify the fractional removal of nitrate as a function of time (t) as

$$F_R^*(t)=\frac{\alpha t}{1+\alpha t} \tag{11}$$

where α is a constant first-order decay rate (day^{-1}). Equation (11) gives the cdf for fractional nitrate removal (i.e. $F_R^*(t=\infty)=1$). We weight equation (11) by the exposure time distribution of the domains as

$$F_R(t)=\int_0^t (E\cdot F_R^*)(\tau)\,d\tau \tag{12}$$

where $(E\cdot F_R^*)(\tau)=E(\tau)\cdot F_R^*(\tau)$ is the point-wise product of the two functions. This operation yields a distribution of fractional nitrate removal as a function of time that is dependent only on the exposure time and

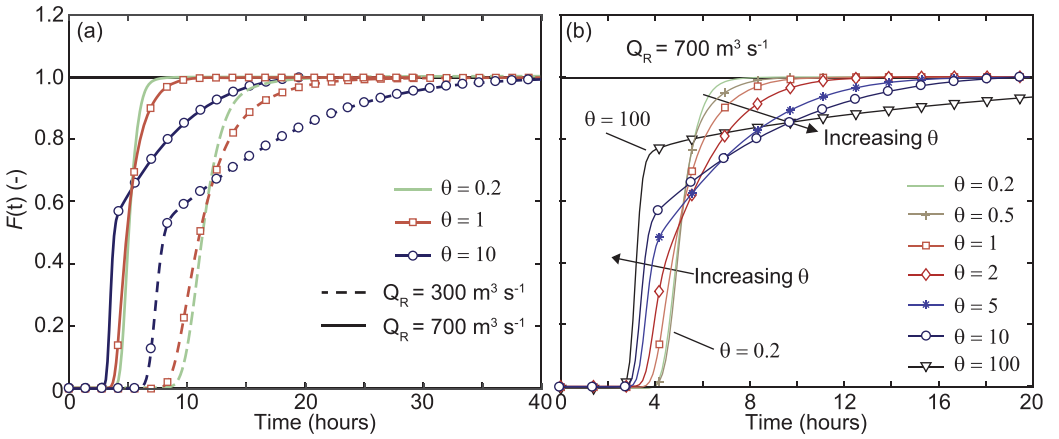

Figure 3. (a) Representation of the ETD in the form of cumulative distribution functions ($F(t)$). Various values of θ are tested. In this case, only $\theta = 0.2$, 1, and 10 are shown for clarity, but the trends for the θ values not shown follow those pictured. (b) $F(t)$ for the $Q_R = 700$ m^3 s^{-1} case for the set of tested θ values. The $\theta = 100$ model run is not completely shown for visualization purposes and comparison with the other runs. $F(t)$ for $\theta = 100$ reaches unity at about 40 h.

the first-order decay rate. The distribution can be partitioned into the contributions from the channel and island portions of the domain. A spatial distribution of nitrate removal $F_R(x_1, x_2, t)$ can be generated by substituting $E(x_1, x_2, t)$ for $E(t)$ in equation (12) and evaluating it at each grid cell in the test domain. We use this model to show the relative contributions of the channels and islands to the system nitrate removal and to highlight hot spots of nutrient removal potential based on the exposure time.

We use equation (11) to calculate α values based on average values of F_R^* and freshwater residence time from studies in estuaries and coastal wetlands (Cheng & Basu, 2017; Dettmann, 2001; Yu et al., 2006). Based on that calculation, we test $\alpha \in = \{0.01, 0.1, 1, 10\}$ day^{-1} as range of representative values. Each α value is held constant in both time and space for each model run. We calculate the spatial distribution of F_R and the relative contributions of channel and islands for each temporally and spatially constant α value. Our range of tested α values represents a variety of coastal aquatic landscapes. While large, deep surface water systems like estuaries and bays have α values on the order of 0.01 or 0.1 day^{-1} (e.g., Dettmann, 2001), shallow wetland systems can have first-order removal rates that are orders of magnitude larger (e.g., Cheng & Basu, 2017; Yu et al., 2006).

3. Results

3.1. Channel-Island Complex

We test the effects of river discharge and island vegetative roughness on ETD in the CIC model. Exposure times associated with $Q_R = 300$ m^3 s^{-1} are expectedly longer than those associated with $Q_R = 700$ m^3 s^{-1} (Figure 3a). A lower discharge leads to a lengthening of the right tail, measured by an increased interquartile range (IQR) as compared to the higher discharge case (Table 2). The interquartile ratio, defined as the

Table 1
Parameters for Numerical Modeling

Symbol	Variable	Value (CIC)	Value (WLD)
Δx_i (m)	Grid size	50	50
Δt (s)	Time step	25	25
$C_{R,1}$	Drag coefficient in channel(s)	0.005	0.005
$C_{R,2}$	Drag coefficient in islands	0.001–0.5	0.005
A_n	Tidal amplitude	0	Equation (6)
Q_R (m^3 s^{-1})	River discharge	300 and 700	3,300
α (d^{-1})	Nitrate removal rate	0.01–10	0.01–10
κ_e (m^2 s^{-1})	Eddy diffusivity	0.01	0.01
ν_e (m^2 s^{-1})	Eddy viscosity	0.01	0.01

Table 2
Summary of ETD Statistics for $Q_R = 300$ and 700 $m^3\ s^{-1}$ in the CIC Model

θ	Median (h)	IQR (h)	$\frac{\text{IQR}}{\text{Median}}$
$Q_R = 300\ m^3\ s^{-1}$			
0.2	11.34	1.94	0.17
1	11.06	3.10	0.28
10	8.14	8.02	0.98
$Q_R = 700\ m^3\ s^{-1}$			
0.2	5.04	0.85	0.17
0.5	5.06	0.78	0.15
1	4.94	1.38	0.28
2	4.89	2.37	0.48
5	4.28	3.43	0.80
10	3.79	3.86	1.02
100	3.28	0.76	0.23

IQR divided by the median, is consistent across Q_R values (Table 2), indicating that Q_R does not affect the relative dispersion of the ETD.

The shape of fractional mass flux curves for the channel ($e_1(t)$) and islands ($e_2(t)$) provides insight into the timing, duration, and magnitude of water flux to the island. In general, the area under $e_2(t)$, or the percentage of tracer allocated to the island, decreases with increasing θ (Figure 4a). The $e_2(t)$ peak height decreases as θ increases, while the $e_1(t)$ peak becomes increasingly pronounced as more water is conveyed by the channel (Figure 4a). In general, the peak of $e_1(t)$ precedes the peak of the $e_2(t)$ because the channel velocities are higher than island velocities. For $\theta = 0.2$, the behavior is reversed (Figure 4a) because the island velocities exceed those of the channel. As θ increases, the median of the total ETD decreases and the tail lengthens (seen as an increase in IQR in Table 2), indicating that the extreme values of the ETD increase. The IQR for $\theta = 100$ is lower than for $\theta = 10$, since most of the distribution mass is concentrated within the peak.

While increased island roughness causes lengthening of the ETD tail, it does not affect the total fraction of nitrate removed from the system (Figure 4b). The F_R distribution becomes more dispersive as θ increases, due to the longer tail in the island mass flux. Lower values of α result in lower values of $F_{R,weighted}$ in all cases. The α=0.01 and 0.1 day^{-1} cases result in very little nitrate removal for all the scenarios tested. Although $F_{R,Total}$ is unchanged across θ values, the relative contributions of the channel and island portions ($F_{R,1}$ and $F_{R,2}$, respectively) are affected (Figure 4b). As θ increases, the island contribution to F_R decreases, since less tracer is allocated to this portion of the domain. For $\alpha = 1\ day^{-1}$, the percentage contributions of nitrate removal owing to time spent within the island range from 83% to 35% for low to high values of θ, respectively.

3.2. Wax Lake Delta

In order to characterize the spatial variability of the water transport time scale, particle tracers were released at each grid cell in the WLD domain for various tidal conditions and the ETD was generated for each tracer

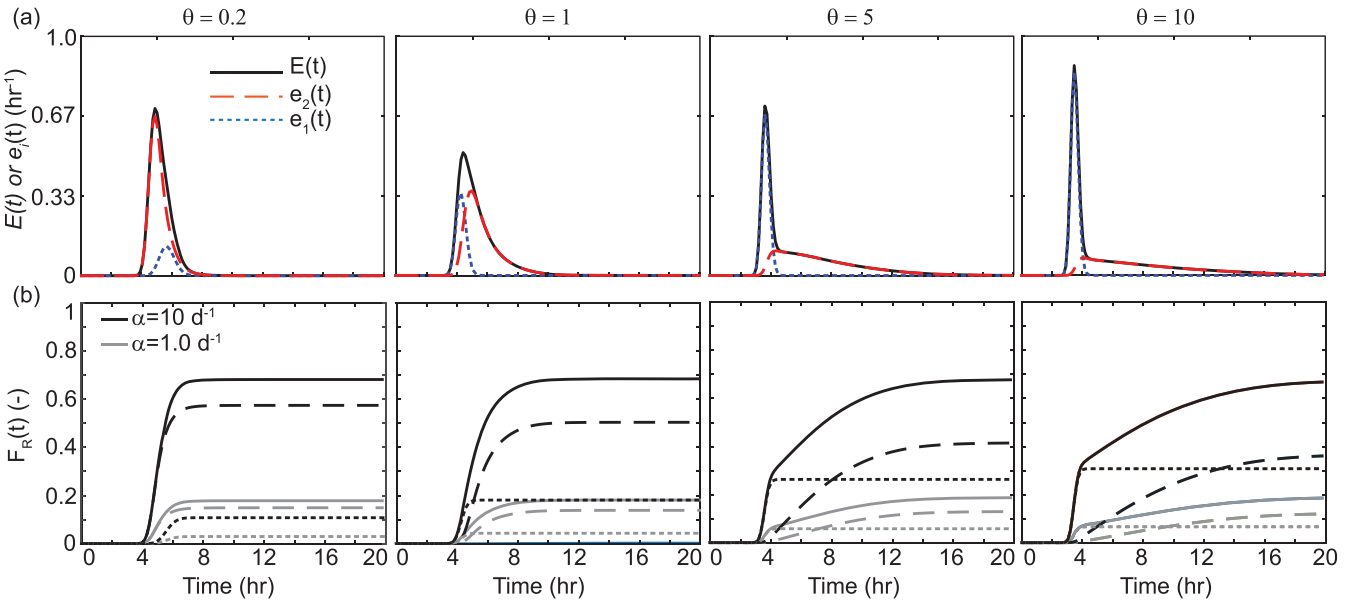

Figure 4. Summary of ETD and nitrate removal for $Q_R = 700\ m^3\ s^{-1}$ in the CIC model. The ETDs are quantified with probability density functions ($E(t)$) and the fractional mass fluxes for channels and islands ($e_i(t)$). (a) ETD for various values of θ. Increases in θ cause decreases in the fraction of water entering the island (represented here by the area under $e_2(t)$). (b) Cumulative fractional nitrate removal for various values of α calculated with equation (12). The contributions of both the channel (dots) and the islands (dashes) are given in relation to the total distribution of fractional nitrate removal. The values for α=0.01 and α=0.1 are not shown because they both yield negligible values of $F_R(t)$ (<0.05).

release location (Figure 5). The spatial variability of the ETD at WLD is well represented by the median exposure time since ETDs have sharp peaks concentrated about the median, indicating that advection tends to dominate the propagation of particles. In all cases, the median exposure time is generally shorter within the channels than in islands due to the relatively high flow velocity associated with the channel flow. The longest median exposure times for each model scenario are associated with relatively high elevation island margins in the northernmost WLD islands (Figure 5). In general, the island margins have longer median exposure times than do the channels or the island interiors. Areas within channels and upstream of island tips tend to have high median exposure times.

Significant variability exists among the various tracer release times (Figure 5). The case forced by the river only has the longest median exposure times, which tend to be concentrated in the northernmost islands. In both the spring and neap tide scenarios, the low tide tracer releases produce the most striking difference in median exposure time between the channels and the islands. The low tide tracer runs also have generally longer median exposure times than the other scenarios. This result is expected, because low tide immediately precedes rising tide, which produces a flood tidal current and landward flow. High and rising tide tracer releases tend to be associated with spatially uniform median exposure times, although the

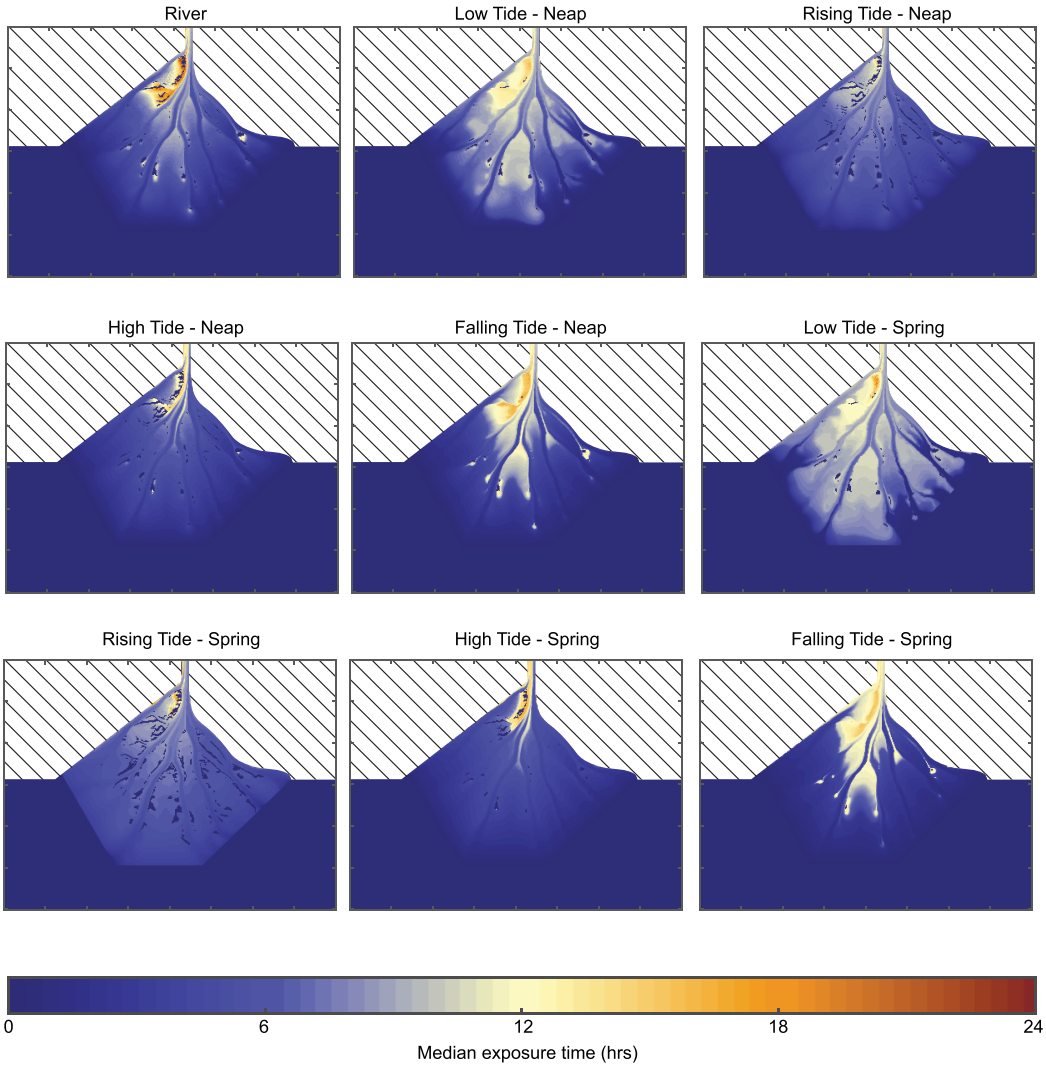

Figure 5. Spatial maps of median exposure times for various tidal scenarios. The labels indicate the tidal condition at the time of the tracer release. The highest median exposure times are generally found within the upstream portions of the islands, along the island margins, and near the delta apex. Areas with median exposure times of 0 h represent locations that were not inundated at the time of tracer release.

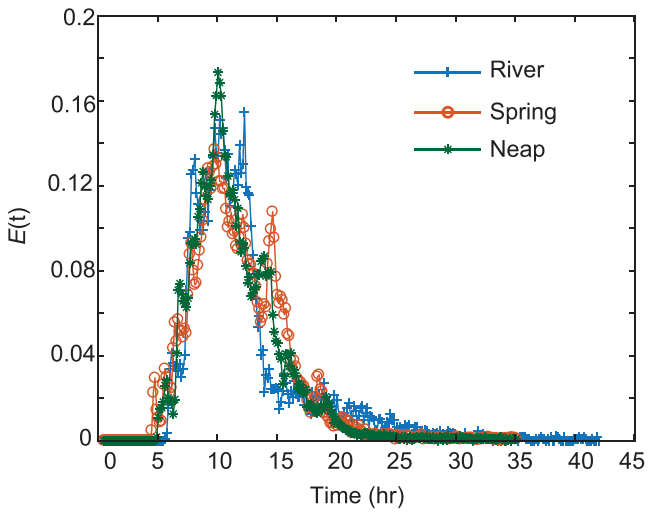

Figure 6. Comparison among the ETDs for the river, spring tide, and neap tide scenarios. The spring and neap tide distributions are combined exposure time distributions across the four tidal release times (high, falling, low, and rising). The distributions are statistically similar at the 5% significance level according to Wilcoxon rank-sum tests (river-spring, $p = 0.06$; river-neap, $p = 0.22$; spring-neap, $p = 0.48$). The low p-value for the river-spring comparison is likely due to the secondary peak in the Spring $E(t)$ at around 15 h.

northernmost islands still tend to have distributions with relatively large medians (Figure 5). In general, there is little difference between the magnitudes and the spatial distribution of spring and neap exposure time medians.

The system ETD for WLD is quantified by releasing particle tracers at the delta apex (upstream boundary in Figure 1e) and monitoring the exposure time within the boundary x_b. The particle tracers released at the apex produce mass flux curves that are statistically similar to those generated with a diffusive tracer (supporting information). The ETD for the river-only model run ($A = 0$ m) has a median exposure time of about 10 h (Figure 6). For spring and neap tides, exposure times for each release within the tidal cycle (high, low, rising, and falling) are amalgamated to create representative distributions for the spring and neap phases of the tidal cycle. The ETDs for river-only, spring tide, and neap tide are statistically similar at the 5% significance level according to Wilcoxon rank-sum tests (p-values: 0.48 for neap-spring, 0.22 for river-neap, and 0.06 for river-spring), indicating that tides do not significantly affect the system-scale ETD at WLD. We note that the river-spring comparison barely passes the rank-sum test at a 5% significance level, which may be due to a secondary peak in the spring tide ETD at a median exposure time of 15 h (Figure 6).

Since median exposure times associated with the islands are generally longer than in the channels (Figure 5), it would be beneficial to understand how the time spent in the islands compares to the exposure time in the entire system. To quantify the contribution of island exposure times to the system exposure times, we calculate the island ETD by counting the cumulative time a tracer spends within island boundaries (Figure 1e) and introduce the Island Exposure Index (IEI) as ratio of the median island exposure time to the median exposure time (Figure 7). The IEI is the fraction of a tracer particle's median exposure time that is spent within the island boundaries. The spatial distribution of IEI is consistent among the different model runs, suggesting that tides have little effect on the hydrological exchange between channels and islands (Figure 7). Large islands near the system boundary tend to have IEI values near unity, indicating that once a water parcel enters the island, it remains there until exiting the system entirely. Channels near the system boundary tend toward IEI = 0, indicating that tracer particles flowing through these areas generally do not enter an island. However, the more upstream channels tend to have higher values of IEI, because tracer particles originating closer to the apex have higher probabilities of travel through the islands than do tracer particles released in channels near the system boundary. The value of IEI at the delta apex is 0.37−0.50 across all of the cases tested, indicating that roughly one third to one half of the median exposure time is due to transport within the delta islands.

The cumulative fraction of nitrate removal, $F_{R,Total}$, is a function of only the ETD and the decay rate α. Accordingly, the spatial pattern for $F_{R,Total}$ is correlated with that of the ETD. The spatial differences in $F_{R,Total}$ clearly distinguish the channelized portions of WLD from the islands (Figure 8) in accordance with the ETD results. The largest values of $F_{R,Total}$ are generally found in the more landward portions of the islands and along island margins (Figure 8). Areas of the channel associated with relatively high values of $F_{R,Total}$ are generally found directly upstream of island apices (e.g., Falling Tide-Neap in Figure 8) and are associated with high values of IEI (Figure 7). Relatively high values of $F_{R,Total}$ are found near the apex of the delta, since particles passing through the apex are likely to traverse an island, which has relatively slow transport leading to greater removal. The fractional nitrate removal associated with water parcels passing through channels is generally less than 0.2, but $F_{R,Total}$=0.28−0.31 for the water parcels passing through the delta apex for $\alpha = 1$ day^{-1}.

4. Discussion

4.1. Exposure Time Distributions and Hydrological Connectivity

This study represents the first attempt, to our knowledge, at quantifying network-scale surface water ETD in a coastal river delta. We presented a modeling analysis of various environmental controls on ETD in the

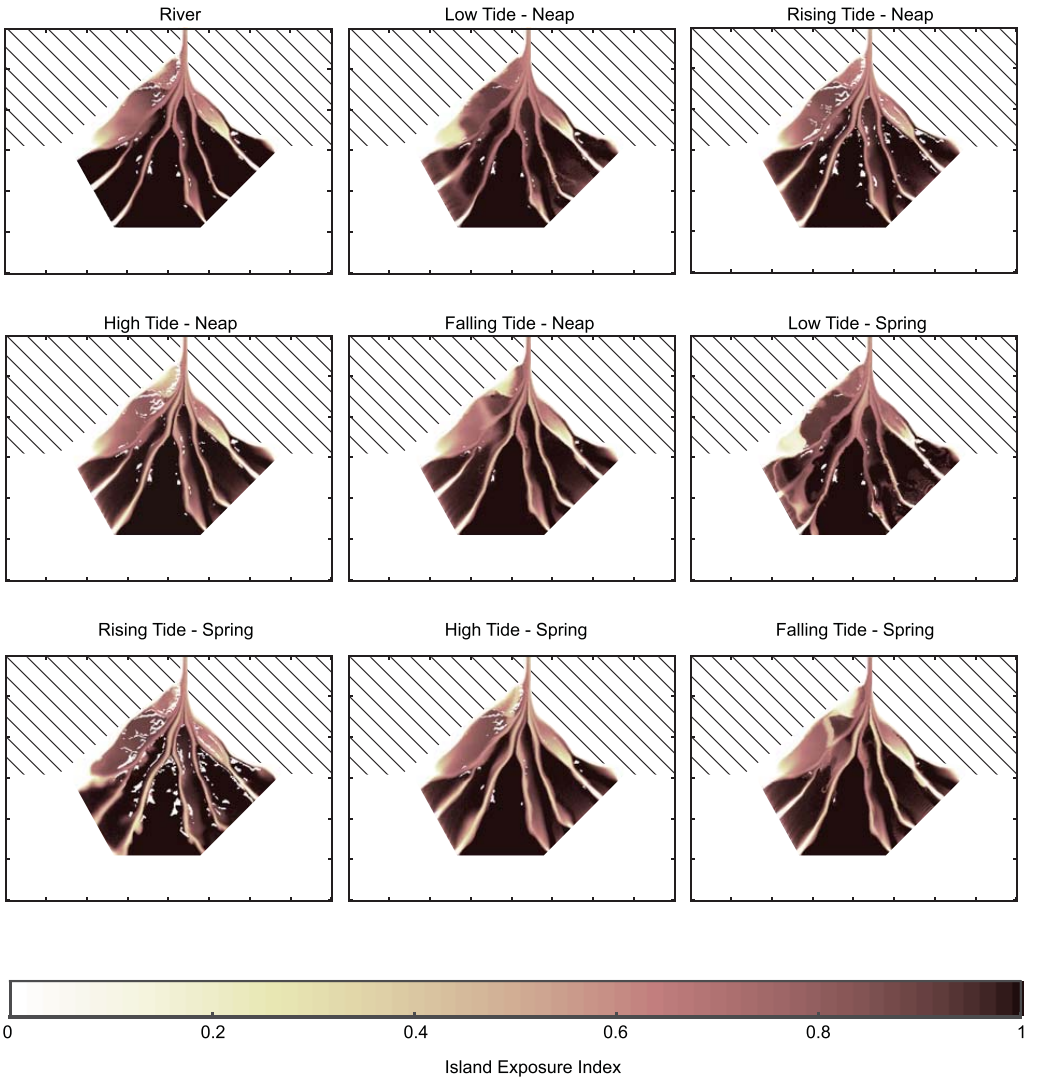

Figure 7. Spatial maps of the Island Exposure Index (IEI), or the fraction of the median island exposure time and the median exposure time. The labels indicate the tidal condition at the time of the tracer release. High IEI values are found within the island interiors. The IEI near the delta apex is relatively high compared to more downstream portions of the channels, since water parcels near the delta apex have a higher probability of passing through the islands. White areas within islands represent locations that were not inundated at the time of tracer release.

simplified CIC and the full WLD domains. We quantified the roles of vegetation roughness within the islands and river discharge with the CIC model, and the roles of tides and network structure with the WLD model. We find HC between channels and deltaic islands, and the retaining capacity of the islands, to be primary controls on the ETD.

The hydraulic roughness of lateral vegetated zones like the islands in the CIC model controls the allocation of flow between channels and vegetated zones (Hiatt & Passalacqua, 2017; Musner et al., 2014), which impacts the ETD. In the CIC model, median exposure time decreases as the percentage of flow allocated to the islands increases (Figure 9). As vegetation roughness increases, the local velocity within vegetated zones decreases (Nepf, 2012), which naturally leads to increased exposure times within the vegetated zone. However, since increasing vegetation roughness decreases lateral outflow from the channel to the islands (Figure 9), the ETD is increasingly dominated by the channel portion of the signal (Figure 4a), due to increased velocities within the channel (Hiatt & Passalacqua, 2017; Musner et al., 2014; Temmerman et al., 2007; Vandenbruwaene et al., 2011). Increased vegetation within delta islands is likely to lead to a reduced HC and fast transport within the channels, reducing the exposure time. This result points to the importance of

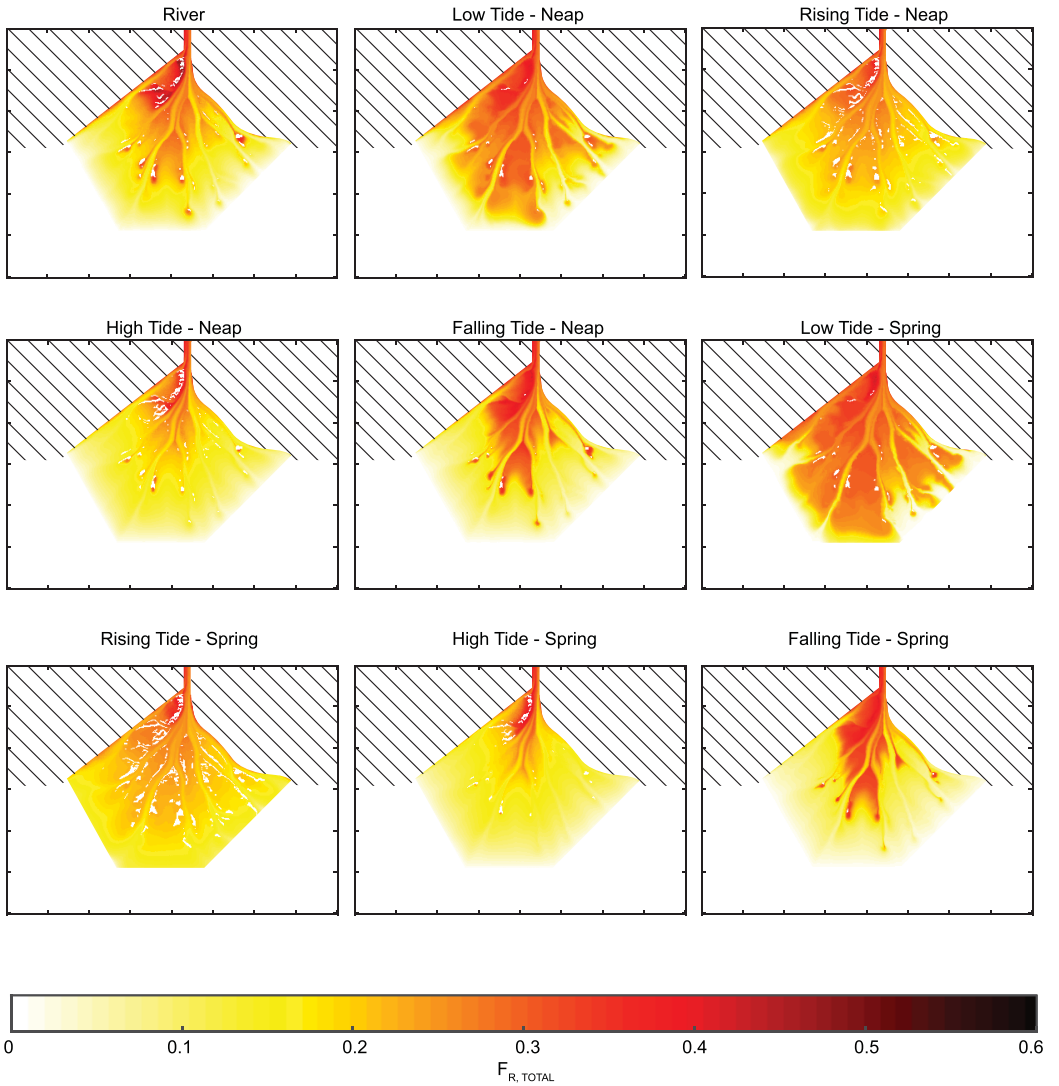

Figure 8. The total fractional nitrate removal associated with ETD and $\alpha = 1$ day^{-1}. The $F_{R,total}$ value can be interpreted as the fractional removal associated with water passing through that cell, although the removal may occur elsewhere in the domain. The labels indicate the tidal condition at the time of the tracer release. Significant variability exists among the different scenarios, but high values of $F_{R,total}$ are found near the delta apex and throughout the islands. White areas within islands represent locations that were not inundated at the time of tracer release.

considering so-called reach-scale flow interaction with vegetation (Luhar & Nepf, 2013; Nepf, 2012) when assessing water transport time scales in wetland and deltaic ecosystems.

We observe differences between modeled water transport time scale distributions between a treatment wetland similar to the CIC (Musner et al., 2014) and the CIC results. Bimodal residence time distributions (equivalent to ETD, in this case) have been quantified for treatment wetlands with a single main flow channel with lateral vegetated zones (Musner et al., 2014). While our modeling setup is similar to that of Musner et al. (2014), we did not identify bimodal ETDs in our CIC model (Figure 4a). The lack of bimodality is likely due to the relatively high-velocity flow in the channel as compared to those tested in Musner et al. (2014), which renders the CIC an advection-dominated system, causing the distribution to be concentrated around the median exposure time for the channel flow (e.g., Figure 4a). With decreasing discharge, we still do not observe a bimodal distribution, but the influence of the island on the tail of the ETD is more strongly felt (Figure 3a). Discharge fluctuations at WLD on a longer time scale than the time scales of the calculated ETDs (Sendrowski & Passalacqua, 2017) and our assumption of constant discharge is thus adequate for the time scales considered. While river discharge obviously influences the nominal values of the ETD, it may

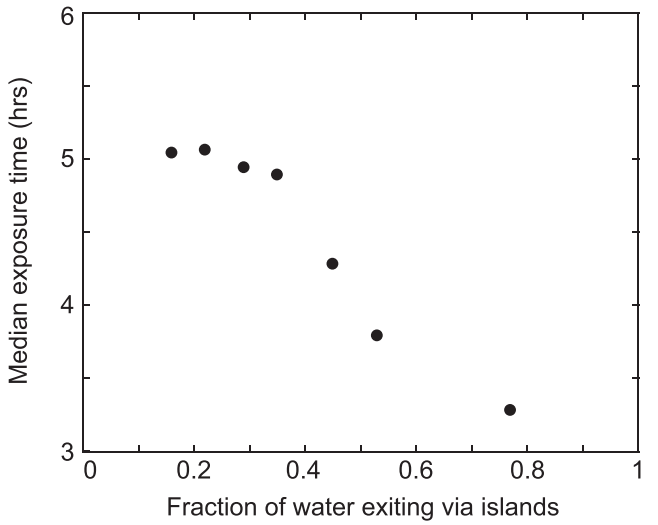

Figure 9. The percentage of discharge exiting the system via the islands is related to the median exposure time in the CIC model.

have a limited role on its overall shape in a river delta with strong riverine influences, since the fraction of lateral outflow from channels to islands in the backwater zone is insensitive to changes in river discharge for nonflood conditions (Hiatt & Passalacqua, 2017).

We propose that the spatial trend in ETD within the island is related to the HC between the channel and the island. Channels allocate a significant percentage of their flow to the island interiors at WLD, but the location of that lateral outflow also depends on levee elevation, vegetation, and secondary channels connecting to the island interiors (Hiatt & Passalacqua, 2015, 2017). Since the more landward portions of the islands have relatively high elevation (Wagner et al., 2017), they tend to receive less flow from the channel, leading to longer exposure times (Figures 5 and 8). Further seaward, as levee elevation decreases (Wagner et al., 2017), lateral outflow from the channel increases velocities within the island (Hiatt & Passalacqua, 2015, 2017), which reduces the exposure time. However, even though increasing vegetation roughness decreases the fraction of flow allocated to the islands (Hiatt & Passalacqua, 2017; Musner et al., 2014), exposure times increase because of water transport within islands (Figure 4). Thus, the increased roughness owing to the presence of vegetation in islands acts to locally increase but globally decrease exposure times. This competition is important to consider for the management of river diversion projects that seek to reduce nutrient delivery to the coast, which is, for example, a major focus of the Louisiana Coastal Master Plan (LCPRA, 2017).

While WLD is generally considered a prototypical river-dominated delta, tides have been shown to affect the evolution of its distributary channels (Shaw & Mohrig, 2014) and system inundation dynamics (Geleynse et al., 2015; Sendrowski & Passalacqua, 2017). However, our analysis shows that, under average flow conditions ($Q = 3{,}300\ m^3\ s^{-1}$), tides have little effect on the ETD at the system scale, similar to other systems (Viero & Defina, 2016). Although tracers released at different water levels during the semidiurnal tidal cycles yield differences in the spatial distribution of median exposure times (Figure 5), the ETDs for flow entering through the delta apex are unaffected by tides (Figure 6). Tides also do not significantly affect the IEI, indicating that network-scale HC between channels and islands is generally unaltered by tides at WLD.

Water transport time scales can be influenced by enhanced diffusion processes due to complex bathymetry in coastal systems (Cucco & Umgiesser, 2006; Umgiesser et al., 2014; Viero & Defina, 2016), but the transport at WLD may be dominated by the lack of network complexity (Tejedor et al., 2015a, 2015b), resulting in the apparent control of advective processes on ETD (Figure 6). A simple network structure allows a water parcel to follow only a few alternative paths before exiting the system, which is typical of a relatively young deltaic system (Tejedor et al., 2016). As the number of alternative paths through a network increases, the dispersion of the ETD will likely increase, especially if there is significant channel-island HC. However, elevation in deltaic islands tends to approach an equilibrium (Wagner et al., 2017) that may lead to decreasing frequency of inundation (Marani et al., 2010). Quantifying the changes in water transport time scales as a function of the morphological development of a river delta remains an open area of research.

4.2. Implications for Nutrient Removal

The network of channels and hydrologically connected islands in a river delta may lead to significant spatial variability in nutrient removal capabilities, which can cause challenges for using local estimates at the network level. Since nitrate removal rate is a function of water transport time scales (Cheng & Basu, 2017; Dettmann, 2001; Nixon et al., 1996; Yu et al., 2006), quantifying ETDs in a river delta represents an important step forward. Our work helps identify locations, based on ETD, IEI, and degree of HC with the channel, that are potential hot spots for nutrient cycling at WLD.

Coupled with the result that roughly half of the flow at WLD enters the islands (Hiatt & Passalacqua, 2015, 2017; Shaw et al., 2016a) and the island exposure time generally comprises a significant portion of the system exposure time (Figure 7), we find that nitrate removal within deltaic islands accounts for 52–73% of the total nitrate removed (Figure 11a) for α values ranging 4 orders of magnitude. This result indicates that the

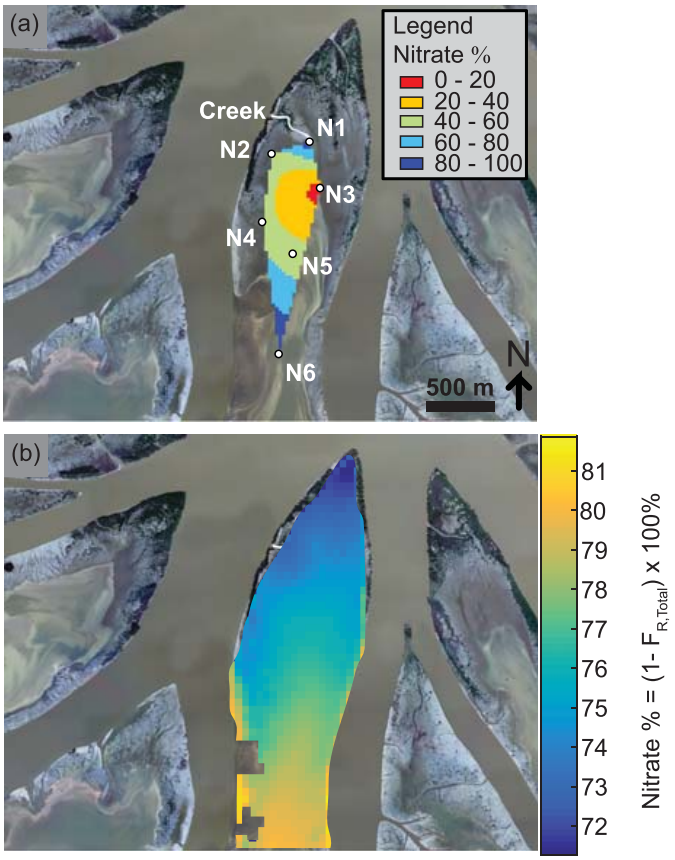

Figure 10. Summary of the nitrate concentration measurements from Mike Island in spring 2015. (a) Locations of the SUNA stations measuring nitrate concentration on Mike Island with a spatially interpolated grid of average nitrate percentage (concentration at location divided by influx concentration). (b) Snapshot of the total nitrate percentage $(1 - F_{R,Total})\cdot 100\%$ for the same area in the river-only model run ($A = 0$ m) with $\alpha = 1$ day^{-1}. While the magnitude of removal generated by the model does not match those observed at WLD, the model does capture the broad spatial patterns of fractional nitrate removal, with higher values of $F_{R,Total}$ occurring in the northern portion of the island, and decreasingly lower values in the more southern portion.

WLD islands are not only the likely location for nutrient removal to occur (Henry & Twilley, 2014), since the water exposure time is relatively high, but that a large fraction of the incoming water discharge reaches these zones where dissolved nitrate may be processed. A majority of the removal is owed to time spent within the islands, regardless of the tidal conditions (Figure 11b). By quantifying ETDs along with the volume of water delivered to the island interiors, our study establishes links among the network-scale delta hydraulics, channel-island HC, and nutrient removal. Previous studies have focused on accurately quantifying nitrate removal rates and spatially integrated nitrate removal fractions in delta islands (Henry & Twilley, 2014) and diversion wetlands (DeLaune et al., 2005; Lane et al., 1999, 2003), often using simple measures for water transport time scales (e.g., Cheng & Basu, 2017; Yu et al., 2006). We propose that estimates of nutrient removal in river deltas must explicitly account for the channel-island HC in order to adequately estimate network-scale ETD, and, subsequently, nitrate removal.

While our nutrient model ignores many of the complexities of nutrient transformation processes in wetlands, we test its ability to reproduce observed nutrient removal fractions in the field. We measured surface water nitrate concentrations at Mike Island (Figure 10a) from 1 April 2015 to 11 June 2015 (two sensors began recording in May). Six submersible ultraviolet nitrate analyzers (SUNA) measured ambient nitrate concentrations at 1 h intervals in the wetland water column along the upstream-downstream gradient in Mike Island. Each hourly data point is an average of thirty seconds of continuously measured nitrate concentrations. Nitrate data are presented as spatially interpolated mean concentrations (Figure 10a) for the entire time series. Location N1 provides an upstream boundary condition because it is directly connected to the main distributary channel through a secondary channel that flows into the interior of the island; N1 is located 400 m from the mouth of the secondary channel. Taking the mean concentration at N1 as the baseline concentration from which to calculate fractional removal of nitrate, locations N2, N3, N4, and N5 show nitrate removal fractions of 0.47, 0.91, 0.55, and 0.52, respectively. Location N6 has concentrations that are similar to N1, which is due to the channel-island connectivity near the sensor that introduces significant inflow from the main channel.

Our simple model does not reproduce the nitrate removal fractions observed within Mike Island at the chosen value of α, but identifies the general spatial trends of nitrate removal in a morphologically and hydraulically heterogeneous network. Higher values of $F_{R,Total}$ are generally found in the northern portion of the island and values generally decrease moving seaward (Figure 10b), which is also the case in the field (Figure 10a). The northern portion of the island (edges: N2–N4) is characterized by shallow areas with emergent vegetation that decrease water flow, leading to higher exposure times and nitrate removal, which may be due to plant uptake and microbial activity (Kadlec, 2012). In contrast, locations N5 and N6 are located in the central deeper section of the island, where higher water velocities limit nitrate removal due to less exposure time within the island (Castañeda Moya et al., 2015). The discrepancy between the modeled nutrient removal and the observed concentrations is likely due to the simple parameterization of the first-order decay rate α. We note that while the model does not produce the same magnitude of nutrient removal as observed in the field, a pattern of high to low nitrate removal moving landward to seaward is detected in the modeled and observed results. This pattern is likely related to soil age and organic matter content in the WLD islands (Henry & Twilley, 2014) and correlates with established hydrogeomorphic zones that are defined by soil elevation and vegetation (Bevington & Twilley, 2018).

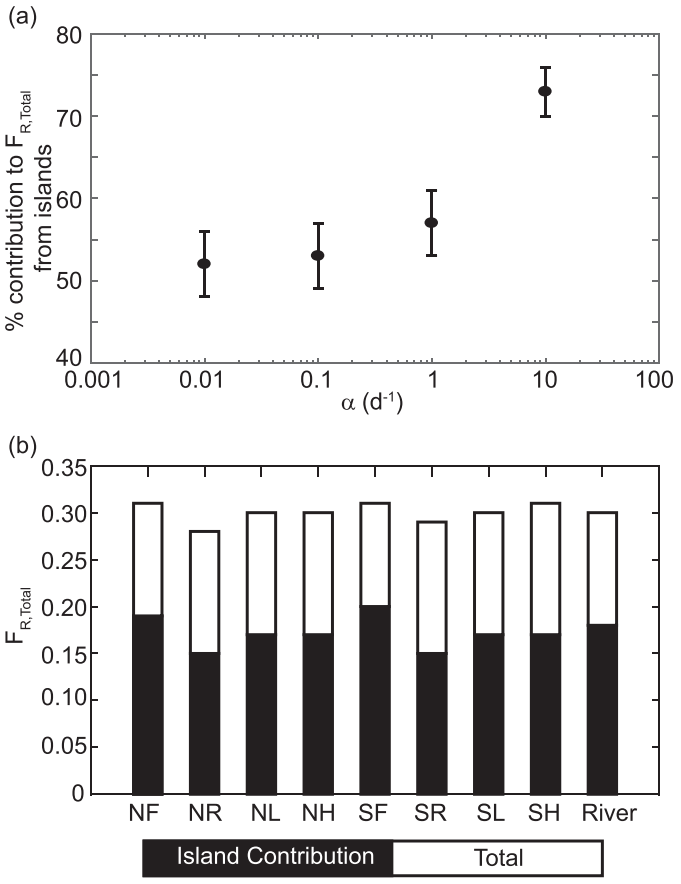

Figure 11. Summary of the island contribution to $F_{R,Total}$ in the WLD model runs. (a) The average percent contribution across model runs of nitrate removal owing to time spent in the WLD islands. In each case, more than half of the nitrate removal is due to time spent within islands and the relative contribution increases with increasing α. The error bars represent the standard deviation about the mean. (b) The total fraction of nitrate removed ($F_{R,Total}$) for water parcel passing through the apex in each WLD model run with $\alpha = 1$ day^{-1}. The contribution of the islands to $F_{R,Total}$ is also displayed. The differences in tidal conditions have little influence on both $F_{R,total}$ and the contribution owing to the islands. The acronyms indicate the tidal condition at the time of the tracer release (N, neap; S, spring; F, falling; R, rising; L, low; H, high; River, no tides).

Modeled exposure times were <48 h and the WLD median exposure time was roughly 10 h for all cases tested. Most work on linking water transport time scales to nutrient removal in coastal systems like estuaries and bays indicates that much longer time scales (order of weeks to months) are necessary to produce significant nutrient removal (e.g., Dettmann, 2001; Nixon et al., 1996; Perez et al., 2003). In wetlands, nutrient removal can be achieved within shorter time scales (Cheng & Basu, 2017; Yu et al., 2006) and delta islands at WLD behave similarly to coastal wetlands in terms of nutrient removal (Henry & Twilley, 2014). While it is difficult to constrain the first-order removal rate at WLD with the available data, the results obtained are qualitatively comparable to those in relatively similar and nearby systems. Estimates from the nearby Davis Freshwater Pond diversion indicate that nitrate removal efficiencies of about 42% are possible for water transport times of 24 h, which translates to α=0.72 day^{-1} according to equation (11). Our model predicts a system-wide removal efficiency of about 30% for $\alpha = 1$ day^{-1} (Figure 11) for a median exposure time of about 10 h. A recent survey of aquatic systems world wide indicates that both natural and constructed wetlands can host first-order removal rates ranging from about 10^{-4} to 10^{2} day^{-1} for water residence times ranging from 10^{2} to 10^{-2} day, respectively (Cheng & Basu, 2017); our results lie within these ranges. Nevertheless, accurate estimates of the magnitude of nutrient removal require more complex nutrient biogeochemistry models than presented in this study.

4.3. Limitations and Directions for Future Research

This study does not address the potentially important effects of vegetation patches on water transport. We applied vegetation roughness uniformly over the island surface in the CIC model, but vegetation patterns are more complex in the field (Carle et al., 2013). Vegetation patches have been shown to produce more complicated flow patterns through coastal marshlands (Bouma et al., 2009; Larsen et al., 2017; Temmerman et al., 2007; Vandenbruwaene et al., 2011), and likely have an impact on the ETD due to a more complex pattern of HC. Although the WLD model can produce realistic channel hydraulics and channel-island HC (Hiatt & Passalacqua, 2017), the lack of vegetation within the island interiors likely causes ETD estimates to be shorter than in reality both locally and at the network scale. Tracer studies from the field indicate that increased transport time associated with transient storage in and near vegetation patches is significant (Hiatt & Passalacqua, 2015).

Wind has been ignored in this analysis but can affect water circulation in coastal systems (Feng & Li, 2010; Walker & Hammack, 2000; Roberts et al., 2015). For example, in Fourleague Bay, nearby WLD, northerly winds associated with cold fronts can flush up to 56% of the bay volume and reduce the flushing time (Perez et al., 2003). Further, Roberts et al. (2015) have reported wind-induced increases in water levels (up to 1 m) inside bays in the Atchafalaya-WLD region as cold fronts approach. Similar behavior may be relevant to ETDs in deltaic systems since winds can influence island inundation dynamics (Geleynse et al., 2015; Sendrowski & Passalacqua, 2017). Quantifying the influence of wind on HC and water transport times scales in river deltas remains an open research topic.

Our study does not address the effects of groundwater in channel-island HC. Surface water-groundwater exchange and hyporheic exchange are important components in HC (Bracken et al., 2013) and biogeochemical processing (Gomez et al., 2012). Global-scale estimates of groundwater discharge account for only 6% of the inputs to the sea (Zektser & Loaiciga, 1993), but much of the water entering a delta system is subject to surface-groundwater exchange (Sawyer et al., 2015) and channel-island exchange via groundwater

(O'Connor & Moffett, 2015). To improve estimates of nutrient removal in deltaic systems, future work should look to determine the relative contributions of surface and groundwater to the ETD.

The nitrate removal model used in this study is intentionally simple. The decay rate α is taken to be spatially and temporally constant in order to identify the relative contributions of channels and islands to the overall nutrient removal fraction and to identify hot spots of nutrient removal potential based on network structure at WLD. Though removal rates vary spatially and temporally based on nutrient loading rate and concentration (Lane et al., 2003; Mitsch et al., 2001), temperature (Kadlec, 1999, 2010, 2012), water chemistry (Kadlec, 2012), vegetation (Lane et al., 2003), and wetland age and organic matter content (Henry & Twilley, 2014; Kadlec, 2012), these factors are considered beyond the scope of our analysis. Nevertheless, first-order reaction rates remain useful tools for understanding the influence of water transport time scales on nutrient removal and for efficient upscaling of nutrient removal estimates where detailed models may be unavailable (e.g., Cheng & Basu, 2017).

5. Conclusions

The controls on water exposure time distributions were quantified using hydrodynamic modeling at Wax Lake delta, a naturally prograding delta in Louisiana, USA. The shallow water equations were solved numerically in two dimensions and coupled with advection/diffusion and particle tracers to quantify exposure time distributions under a range of conditions. The controls exerted by river discharge and vegetative drag were quantified for an idealized channel-island complex based on Wax Lake delta bathymetry. The effects of delta network geometry and tides were tested in a model of the Wax Lake delta. Hydrological connectivity between the channels and the islands and the retention capacity of the islands were shown to be primary controls over exposure time distributions and nitrate removal. The results presented in this analysis provide a first step for spatially explicit modeling of water transport time scales in river deltas, which was shown to have promise for identifying hot spots of nutrient removal.

We draw the following conclusions:

1. The exposure time distribution is a function of the hydraulic roughness associated with vegetation in deltaic islands. Increasing hydraulic roughness tends to shorten the median exposure time, due to flow concentration within the primary channel, while extreme values of the exposure time distribution associated with transport within the islands are increased. As vegetative roughness in the islands increases, the contribution of exposure times within the islands to the total system exposure time distribution decreases. Thus, deltaic island vegetation tends to increase local exposure times, while limiting the connectivity with the channel, which leads to decreased exposure times within deltaic channels.
2. Tides have a limited effect on the system exposure time distribution at Wax Lake delta, which is due to the relatively large fluvial input into the system. The median exposure time for water parcels entering the delta through the apex for situations with and without tides was about 10 h.
3. Changes in river discharge do not affect the shape of the exposure time distribution and only modulate the nominal values. River discharge fluctuations do not affect the relative dispersion of the exposure time distribution, since the fraction of flow allocated to islands is unaffected in the subcritical flow in the regime where backwater effects dominate.
4. Water transport through islands constitutes 37–50% of the system exposure time distribution, indicating that hydrological connectivity with delta islands has a significant influence on water transport time scales at Wax Lake delta.
5. Transport within inundated delta islands accounts for 52–73% of the estimated nitrate removal for the whole Wax Lake delta system depending on the chosen α value. Deltaic islands are thus important hot spots for biogeochemical activity. Provided there is significant channel-island hydrological connectivity, islands may account for the bulk of nutrient removal in branching river deltas like Wax Lake delta.

Notation

A_n	tidal amplitude of constituent n, m.
c	tracer concentration, mass m^{-3}.
C_B	bottom drag coefficient.

C_D	cylinder drag coefficient.
C_R	modified Chézy coefficient, $m^{1/2}\ s^{-1}$.
D	diffusion velocity for particle tracer, $m\ s^{-1}$.
$E(t)$	differential exposure time distribution, h^{-1}.
$e_i(t)$	fractional mass flux at location i, h^{-1}.
$E(x_1, x_2, t)$	differential exposure time distribution at location (x_1, x_2), h^{-1}.
$F(t)$	cumulative exposure time distribution.
$F_R(t)$	fractional nitrate removal according to equation (12).
$F_R(x_1, x_2, t)$	fractional nitrate removal at location (x_1, x_2).
$F_R^*(t)$	fractional nitrate removal according to Dettmann (2001).
$F_{R,Total}$	total fraction of nitrate removed.
G_n	tidal phase lag of constituent n, rad.
g	gravitational acceleration, $m\ s^{-2}$.
H	local depth, m.
h_v	vegetation stem height, m.
n	vegetation frontal area per unit volume, m^{-1}.
N	tracer mass, kg or particle number.
N_{Total}	total tracer mass, kg or number of particles.
Pr_t	turbulent Prandtl number.
$q_\perp$	volumetric flow rate per unit length perpendicular to boundary, $m^2\ s^{-1}$.
Q_R	river discharge, $m^3\ s^{-1}$.
t	time.
u_i	depth-average horizontal velocity, $m\ s^{-1}$.
V	magnitude of horizontal speed, $m\ s^{-1}$.
x_B	along-boundary coordinate.
x_i	horizontal directions.
α	first-order decay rate, day^{-1}.
η	free surface elevation, m.
κ_e	scalar diffusivity coefficient, $m^2\ s^{-1}$.
ν_e	horizontal eddy viscosity coefficient, $m^2\ s^{-1}$.
Φ	random number.
σ_n	angular speed of constituent n, $rad\ h^{-1}$.
τ	dummy variable for time, h.
θ	ratio of the island $C_{R,2}$ to the channel $C_{R,1}$.
CIC	channel-island complex.
ETD	water exposure time distribution.
IEI	Island Exposure Index.
cdf	cumulative distribution function.
IQR	inter-quartile range.
pdf	probability density function, h^{-1}.
WLD	Wax Lake delta.

Acknowledgments
This material is based on work supported by the NSF grants CAREER/EAR-1350336 (P.P.), OCE-16002222 (P.P.), and FESD/EAR-1135427 (P.P. and R.T.), Louisiana Sea Grant College Program under NOAA award NA14OAR4170099 (R.T.), NSF-1417433, and CCF-1331610 (B.R.H.), and NSF Graduate Research Fellowship grant DGE-1110007 (M.H.). The authors thank the Editor, Associate Editor, and five anonymous reviewers who helped improve the quality of this paper. The authors extend special thanks to those who assisted in the field efforts at WLD. Thank you to D. Duncan, R. W. Wagner, and B. Minton for collecting and providing a portion of the field data used in the supporting information. The data used are available in an online repository hosted by The University of Texas at Austin accessible via https://utexas.box.com/s/aamjgo018yq9cor3ck1wcc5n1y6vdmhg.

References

Allison, M. A., & Meselhe, E. A. (2010). The use of large water and sediment diversions in the lower Mississippi River (Louisiana) for coastal restoration. *Journal of Hydrology*, *387*(3–4), 346–360. https://doi.org/10.1016/j.jhydrol.2010.04.001

Baptist, M., Babovic, V., Uthurburu, J. R., Keijzer, M., Uittenbogaard, R., Mynett, A., et al. (2007). On inducing equations for vegetation resistance. *Journal of Hydraulic Research*, *45*(4), 435–450. https://doi.org/10.1080/00221686.2007.9521778

Benjamin, M., & Lawler, D. (2013). *Water quality engineering* (1st ed.). Hoboken, NJ: John Wiley.

Bevington, A. E., & Twilley, R. R. (2018). Island edge morphodynamics along a chronosequence in a prograding deltaic floodplain wetland. *Journal of Coastal Research*, https://doi.org/10.2112/JCOASTRES-D-17-00074.1

Bevington, A. E., Twilley, R. R., & Sasser, C. E., & Holm, G. O., Jr. (2017). Contribution of river floods, hurricanes, and cold fronts to elevation change in a deltaic floodplain, northern Gulf of Mexico, USA. *Estuarine, Coastal and Shelf Science*, *191*, 188–200. https://doi.org/10.1016/j.ecss.2017.04.010

Bouma, T. J., Friedrichs, M., Van Wesenbeeck, B. K., Temmerman, S., Graf, G., & Herman, P. M. J. (2009). Density-dependent linkage of scale-dependent feedbacks: A flume study on the intertidal macrophyte Spartina anglica. *Oikos*, *118*(2), 260–268. https://doi.org/10.1111/j.1600-0706.2008.16892.x

Bracken, L., Wainwright, J., Ali, G., Tetzlaff, D., Smith, M., Reaney, S., et al. (2013). Concepts of hydrological connectivity: Research approaches, pathways and future agendas. *Earth-Science Reviews*, *119*, 17–34. https://doi.org/10.1016/j.earscirev.2013.02.001

Brooks, D., Baca, M., & Lo, Y.-T. (1999). Tidal circulation and residence time in a macrotidal estuary: Cobscook Bay, Maine. *Estuarine, Coastal and Shelf Science*, *49*(5), 647–665. https://doi.org/10.1006/ecss.1999.0544

Camacho, R. A., & Martin, J. L. (2013). Hydrodynamic modeling of first-order transport timescales in the St. Louis Bay Estuary, Mississippi. *Journal of Environmental Engineering*, *139*(3), 317–331. https://doi.org/10.1061/(ASCE)EE.1943-7870.0000647

Carle, M. V., Sasser, C. E., & Roberts, H. H. (2013). Accretion and vegetation community change in the Wax Lake Delta following the historic 2011 Mississippi River flood. *Journal of Coastal Research*, *31*(3), 569–587. https://doi.org/10.2112/JCOASTRES-D-13-00109.1

Castañeda Moya, E., Twilley, R., & Snedden, G. (2015). *Surface water hydrology and nitrate dynamics in delta islands of prograding Wax Lake Delta, Louisiana*. Paper presented at CERF 2015: Grand Challenges in Estuarine and Coastal Science: Securing our Future, Coastal and Estuarine Research Federation, Portland, OR.

Casulli, V., & Cattani, E. (1994). Stability, accuracy and efficiency of a semi-implicit method for three-dimensional shallow water flow. *Computers & Mathematics With Applications*, *27*(4), 99–112.

Casulli, V., & Cheng, R. T. (1992). Semi-implicit finite difference methods for three-dimensional shallow water flow. *International Journal for Numerical Methods in Fluids*, *15*(6), 629–648.

Cea, L., Puertas, J., & Vázquez-Cendón, M.-E. (2007). Depth averaged modelling of turbulent shallow water flow with wet-dry fronts. *Archives of Computational Methods in Engineering*, *14*(3), 303–341. https://doi.org/10.1007/s11831-007-9009-3

Cheng, F. Y., & Basu, N. B. (2017). Biogeochemical hotspots: Role of small water bodies in landscape nutrient processing. *Water Resources Research*, *53*, 5038–5056. https://doi.org/10.1002/2016WR020102

Cucco, A., & Umgiesser, G. (2006). Modeling the Venice Lagoon residence time. *Ecological Modelling*, *193*(1–2), 34–51. https://doi.org/10.1016/j.ecolmodel.2005.07.043

Cucco, A., & Umgiesser, G. (2015). The Trapping Index: How to integrate the Eulerian and the Lagrangian approach for the computation of the transport time scales of semi-enclosed basins. *Marine Pollution Bulletin*, *98*(1–2), 210–220. https://doi.org/10.1016/j.marpolbul.2015.06.048

Cucco, A., Umgiesser, G., Ferrarin, C., Perilli, A., Canu, D. M., & Solidoro, C. (2009). Eulerian and lagrangian transport time scales of a tidal active coastal basin. *Ecological Modelling*, *220*(7), 913–922. https://doi.org/10.1016/j.ecolmodel.2009.01.008

de Brauwere, A., de Brye, B., Blaise, S., & Deleersnijder, E. (2011). Residence time, exposure time and connectivity in the Scheldt Estuary. *Journal of Marine Systems*, *84*(3–4), 85–95. https://doi.org/10.1016/j.jmarsys.2010.10.001

de Brye, B., de Brauwere, A., Gourgue, O., Delhez, E. J., & Deleersnijder, E. (2012). Water renewal timescales in the Scheldt Estuary. *Journal of Marine Systems*, *94*, 74–86. https://doi.org/10.1016/j.jmarsys.2011.10.013

DeLaune, R., Jugsujinda, A., West, J., Johnson, C., & Kongchum, M. (2005). A screening of the capacity of Louisiana freshwater wetlands to process nitrate in diverted Mississippi River water. *Ecological Engineering*, *25*(4), 315–321. https://doi.org/10.1016/j.ecoleng.2005.06.001

Delhez, E. J. (2013). On the concept of exposure time. *Continental Shelf Research*, *71*, 27–36. https://doi.org/10.1016/j.csr.2013.09.026

Dettmann, E. H. (2001). Effect of water residence time on annual export and denitrification of nitrogen in estuaries: A model analysis. *Estuaries*, *24*(4), 481–490. https://doi.org/10.2307/1353250

Diaz, R. J., & Rosenberg, R. (2008). Spreading dead zones and consequences for marine ecosystems. *Science*, *321*(5891), 926–929. https://doi.org/10.1126/science.1156401

Edmonds, D., Paola, C., Hoyal, D., & Sheets, B. (2011). Quantitative metrics that describe river deltas and their channel networks. *Journal of Geophysical Research*, *116*, F04022. https://doi.org/10.1029/2010JF001955

Fagherazzi, S., Edmonds, D. A., Nardin, W., Leonardi, N., Canestrelli, A., Falcini, F., et al. (2015). Dynamics of river mouth deposits. *Reviews of Geophysics*, *53*, 642–672. https://doi.org/10.1002/2014RG000451

Feng, Z., & Li, C. (2010). Cold-front-induced flushing of the Louisiana Bays. *Journal of Marine Systems*, *82*(4), 252–264. https://doi.org/10.1016/j.jmarsys.2010.05.015

Geleynse, N., Hiatt, M., Sangireddy, H., & Passalacqua, P. (2015). Identifying environmental controls on the shoreline of a natural river delta. *Journal of Geophysical Research: Earth Surface*, *120*, 877–893. https://doi.org/10.1002/2014JF003408

Gomez, J. D., Wilson, J. L., & Cardenas, M. B. (2012). Residence time distributions in sinuosity-driven hyporheic zones and their biogeochemical effects. *Water Resources Research*, *48*, W09533. https://doi.org/10.1029/2012WR012180

Henry, K., & Twilley, R. (2014). Nutrient biogeochemistry during the early stages of delta development in the Mississippi River deltaic plain. *Ecosystems*, *17*(2), 1–17. https://doi.org/10.1007/s10021-013-9727-3

Hiatt, M., & Passalacqua, P. (2015). Hydrological connectivity in river deltas: The first-order importance of channel-island exchange. *Water Resources Research*, *51*, 2264–2282. https://doi.org/10.1002/2014WR016149

Hiatt, M., & Passalacqua, P. (2017). What controls the transition from confined to unconfined flow? Analysis of hydraulics in a coastal river delta. *Journal of Hydraulic Engineering*, *143*(6), https://doi.org/10.1061/(ASCE)HY.1943-7900.0001309

Hodges, B. R. (2004). Accuracy order of Crank-Nicolson discretization for hydrostatic free-surface flow. *Journal of Engineering Mechanics*, *130*(8), 904–910. https://doi.org/10.1061/(ASCE)0733-9399(2004)130:8(904)

Hodges, B. R. (2014). A new approach to the local time stepping problem for scalar transport. *Ocean Modelling*, *77*, 1–19. https://doi.org/10.1016/j.ocemod.2014.02.007

Hodges, B. R., Imberger, J., Saggio, A., & Winters, K. B. (2000). Modeling basin-scale internal waves in a stratified lake. *Limnology and Oceanography*, *45*(7), 1603–1620. https://doi.org/10.4319/lo.2000.45.7.1603

Hodges, B. R., & Rueda, F. J. (2008). Semi-implicit two-level predictor–corrector methods for non-linearly coupled, hydrostatic, barotropic/baroclinic flows. *International Journal of Computational Fluid Dynamics*, *22*(9), 593–607. https://doi.org/10.1080/10618560802353389

Holm, G. O., & Sasser, C. E. (2001). Differential salinity response between two Mississippi River subdeltas: Implications for changes in plant composition. *Estuaries*, *24*(1), 78–89. https://doi.org/10.2307/1352815

Howes, N. C., FitzGerald, D. M., Hughes, Z. J., Georgiou, I. Y., Kulp, M. A., Miner, M. D., et al. (2010). Hurricane-induced failure of low salinity wetlands. *Proceedings of the National Academy of Sciences of the United States of America*, *107*(32), 14014–14019. https://doi.org/10.1073/pnas.0914582107

Kadlec, R. (1990). Overland flow in wetlands: Vegetation resistance. *Journal of Hydraulic Engineering*, *116*(5), 691–706. https://doi.org/10.1061/(ASCE)0733-9429(1990)116:5(691)

Kadlec, R. H. (1999). Chemical, physical and biological cycles in treatment wetlands. *Water Science and Technology*, *40*(3), 37–44. https://doi.org/10.1016/S0273-1223(99)00417-5

Kadlec, R. H. (2010). Nitrate dynamics in event-driven wetlands. *Ecological Engineering*, *36*(4), 503–516. https://doi.org/10.1016/j.ecoleng.2009.11.020

Kadlec, R. H. (2012). Constructed marshes for nitrate removal. *Critical Reviews in Environmental Science and Technology*, *42*(9), 934–1005. https://doi.org/10.1080/10643389.2010.534711

Kim, W., Mohrig, D., Twilley, R., Paola, C., & Parker, G. (2009). Is it feasible to build new land in the Mississippi River Delta? *Eos, Transactions American Geophysical Union*, *90*(42), 373–374. https://doi.org/10.1029/2009EO420001
Lane, R., Day, J. W., & Thibodeaux, B. (1999). Water quality analysis of a freshwater diversion at Caernarvon, Louisiana. *Estuaries*, *22*(2), 327–336. https://doi.org/10.2307/1352988
Lane, R., Mashriqui, H., Kemp, G., Day, J., Day, J., & Hamilton, A. (2003). Potential nitrate removal from a river diversion into a Mississippi delta forested wetland. *Ecological Engineering*, *20*, 237–249. https://doi.org/10.1016/S0925-8574(03)00043-0
Larsen, L., Ma, J., & Kaplan, D. (2017). How important is connectivity for surface water fluxes? A generalized expression for flow through heterogeneous landscapes. *Geophysical Research Letters*, *44*, 10349–10358. https://doi.org/10.1002/2017GL075432
LCPRA. (2017). *Louisiana's comprehensive master plan for a sustainable coast* (Technical report). Baton Rouge: The State of Louisiana.
Liang, M., Van Dyk, C., & Passalacqua, P. (2016). Quantifying the patterns and dynamics of river deltas under conditions of steady forcing and relative sea level rise. *Journal of Geophysical Research: Earth Surface*, *121*, 465–496. https://doi.org/10.1002/2015JF003653
Liang, M., Voller, V. R., & Paola, C. (2015). A reduced-complexity model for river delta formation—Part 1: Modeling deltas with channel dynamics. *Earth Surface Dynamics*, *3*(1), 67–86. https://doi.org/10.5194/esurf-3-67-2015
Lightbody, A. F., & Nepf, H. M. (2006). Prediction of velocity profiles and longitudinal dispersion in salt marsh vegetation. *Limnology and Oceanography*, *51*(1), 218–228. https://doi.org/10.4319/lo.2006.51.1.0218
Luhar, M., & Nepf, H. M. (2013). From the blade scale to the reach scale: A characterization of aquatic vegetative drag. *Advances in Water Resources*, *51*, 305–316. https://doi.org/10.1016/j.advwatres.2012.02.002
Luhar, M., Rominger, J., & Nepf, H. (2008). Interaction between flow, transport and vegetation spatial structure. *Environmental Fluid Mechanics*, *8*(5), 423–439. https://doi.org/10.1007/s10652-008-9080-9
Luu, T., Garnier, J., Billen, G., Le, T., Nemery, J., Orange, D., et al. (2012). N, P, Si budgets for the Red River Delta (northern Vietnam): How the delta affects river nutrient delivery to the sea. *Biogeochemistry*, *107*(1–3), 241–259. https://doi.org/10.1007/s10533-010-9549-8
Marani, M., D'Alpaos, A., Lanzoni, S., Carniello, L., & Rinaldo, A. (2010). The importance of being coupled: Stable states and catastrophic shifts in tidal biomorphodynamics. *Journal of Geophysical Research*, *115*, F04004. https://doi.org/10.1029/2009JF001600
Meyers, S. D., & Luther, M. E. (2008). A numerical simulation of residual circulation in Tampa Bay. Part II: Lagrangian residence time. *Estuaries and Coasts*, *31*(5), 815–827. https://doi.org/10.1007/s12237-008-9085-0
Mitsch, W. J., Day, J. W., Gilliam, J. W., Groffman, P. M., Hey, D. L., Randall, G. W., et al. (2001). Reducing nitrogen loading to the Gulf of Mexico from the Mississippi River Basin: Strategies to counter a persistent ecological problem. *BioScience*, *51*(5), 373–388. https://doi.org/10.1641/0006-3568(2001)051[0373:RNLTTG]2.0.CO;2
Monsen, N. E., Cloern, J. E., Lucas, L. V., & Monismith, S. G. (2002). A comment on the use of flushing time, residence time, and age as transport time scales. *Limnology and Oceanography*, *47*(5), 1545–1553. https://doi.org/10.4319/lo.2002.47.5.1545
Musner, T., Bottacin-Busolin, A., Zaramella, M., & Marion, A. (2014). A contaminant transport model for wetlands accounting for distinct residence time bimodality. *Journal of Hydrology*, *515*, 237–246. https://doi.org/10.1016/j.jhydrol.2014.04.043
Nardin, W., Edmonds, D., & Fagherazzi, S. (2016). Influence of vegetation on spatial patterns of sediment deposition in deltaic islands during flood. *Advances in Water Resources*, *93*, Part B, 236–248. https://doi.org/10.1016/j.advwatres.2016.01.001
Nepf, H., Ghisalberti, M., White, B., & Murphy, E. (2007). Retention time and dispersion associated with submerged aquatic canopies. *Water Resources Research*, *43*, W04422. https://doi.org/10.1029/2006WR005362
Nepf, H. M. (1999). Drag, turbulence, and diffusion in flow through emergent vegetation. *Water Resources Research*, *35*(2), 479–489. https://doi.org/10.1029/1998WR900069
Nepf, H. M. (2012). Hydrodynamics of vegetated channels. *Journal of Hydraulic Research*, *50*(3), 262–279. https://doi.org/10.1080/00221686.2012.696559
Nepf, H. M., & Vivoni, E. R. (2000). Flow structure in depth-limited, vegetated flow. *Journal of Geophysical Research*, *105*(C12), 28547–28557. https://doi.org/10.1029/2000JC900145
Nixon, S., Ammerman, J., Atkinson, L., Berounsky, V., Billen, G., Boicourt, W., et al. (1996). The fate of nitrogen and phosphorus at the land-sea margin of the North Atlantic Ocean. *Biogeochemistry*, *35*, 141–180. https://doi.org/10.1007/BF02179826
NOAA. (2016). *National Oceanic and Atmospheric Administration (NOAA) tides and currents*. Retrieved from http://tidesandcurrents.noaa.gov
O'Connor, M. T., & Moffett, K. B. (2015). Groundwater dynamics and surface water–groundwater interactions in a prograding delta island, Louisiana, USA. *Journal of Hydrology*, *524*, 15–29. https://doi.org/10.1016/j.jhydrol.2015.02.017
Paola, C., Twilley, R., Edmonds, D., Kim, W., Mohrig, D., Parker, G., et al. (2011). Natural processes in delta restoration: Application to the Mississippi Delta. *Annual Review of Marine Science*, *3*, 67–91. https://doi.org/10.1146/annurev-marine-120709-142856
Passalacqua, P. (2017). The Delta Connectome: A network-based framework for studying connectivity in river deltas. *Geomorphology*, *277*, 50–62. https://doi.org/10.1016/j.geomorph.2016.04.001
Perez, B., Day, J., Justic, D., & Twilley, R. (2003). Nitrogen and phosphorus transport between Fourleague Bay, LA, and the Gulf of Mexico: The role of winter cold fronts and Atchafalaya River discharge. *Estuarine, Coastal and Shelf Science*, *57*, 1065–1078. https://doi.org/10.1016/S0272-7714(03)00010-6
Perez, B. C., Day, J. W., Jr., Justic, D., Lane, R. R., & Twilley, R. R. (2011). Nutrient stoichiometry, freshwater residence time, and nutrient retention in a river-dominated estuary in the Mississippi Delta. *Hydrobiologia*, *658*, 41–54. https://doi.org/10.1007/s10750-010-0472-8
Rivera-Monroy, V., Lenaker, P., Twilley, R., Delaune, R., Lindau, C., Nuttle, W., et al. (2010). Denitrification in coastal Louisiana: A spatial assessment and research needs. *Journal of Sea Research*, *63*, 157–172. https://doi.org/10.1016/j.seares.2009.12.004
Roberts, H. H., DeLaune, R. D., White, J. R., Li, C., Sasser, C. E., Braud, D., et al. (2015). Floods and cold front passages: Impacts on coastal marshes in a river diversion setting (Wax Lake delta area, Louisiana). *Journal of Coastal Research*, 1057–1068. https://doi.org/10.2112/JCOASTRES-D-14-00173.1
Sawyer, A. H., Edmonds, D. A., & Knights, D. (2015). Surface water-groundwater connectivity in deltaic distributary channel networks. *Geophysical Research Letters*, *42*, 10299–10306. https://doi.org/10.1002/2015GL066156
Sendrowski, A., & Passalacqua, P. (2017). Process connectivity in a naturally prograding river delta. *Water Resources Research*, *53*, 1841–1863. https://doi.org/10.1002/2016WR019768
Shaw, J., & Mohrig, D. (2014). The importance of erosion in distributary channel network growth, Wax Lake Delta, Louisiana, USA. *Geology*, *42*, 31–34. https://doi.org/10.1130/G34751.1
Shaw, J., Mohrig, D., & Whitman, S. (2013). The morphology and evolution of channels on the Wax Lake Delta, Louisiana, USA. *Journal of Geophysical Research: Earth Surface*, *108*, 1562–1584. https://doi.org/10.1002/jgrf.20123
Shaw, J. B., Ayoub, F., Jones, C. E., Lamb, M. P., Holt, B., Wagner, R. W., et al. (2016b). Airborne radar imaging of subaqueous channel evolution in Wax Lake delta, Louisiana, USA. *Geophysical Research Letters*, *43*, 5035–5042. https://doi.org/10.1002/2016GL068770

Shaw, J. B., Mohrig, D., & Wagner, R. W. (2016a). Flow patterns and morphology of a prograding river delta. *Journal of Geophysical Research: Earth Surface*, *121*, 372–391. https://doi.org/10.1002/2015JF003570

Shen, J., & Haas, L. (2004). Calculating age and residence time in the tidal York River using three-dimensional model experiments. *Estuarine, Coastal and Shelf Science*, *61*(3), 449–461. https://doi.org/10.1016/j.ecss.2004.06.010

Somes, N. L., Bishop, W. A., & Wong, T. H. (1999). Numerical simulation of wetland hydrodynamics. *Environment International*, *25*(6), 773–779. https://doi.org/10.1016/S0160-4120(99)00058-6

Stelling, G., & Zijlema, M. (2003). An accurate and efficient finite-difference algorithm for non-hydrostatic free-surface flow with application to wave propagation. *International Journal for Numerical Methods in Fluids*, *43*(1), 1–23. https://doi.org/10.1002/fld.595

Tejedor, A., Longjas, A., Caldwell, R., Edmonds, D. A., Zaliapin, I., & Foufoula-Georgiou, E. (2016). Quantifying the signature of sediment composition on the topologic and dynamic complexity of river delta channel networks and inferences toward delta classification. *Geophysical Research Letters*, *43*, 3280–3287. https://doi.org/10.1002/2016GL068210

Tejedor, A., Longjas, A., Zaliapin, I., & Foufoula-Georgiou, E. (2015a). Delta channel networks: 1. A graph-theoretic approach for studying connectivity and steady state transport on deltaic surfaces. *Water Resources Research*, *51*, 3998–4018. https://doi.org/10.1002/2014WR016577

Tejedor, A., Longjas, A., Zaliapin, I., & Foufoula-Georgiou, E. (2015b). Delta channel networks: 2. Metrics of topologic and dynamic complexity for delta comparison, physical inference, and vulnerability assessment. *Water Resources Research*, *51*, 4019–4045. https://doi.org/10.1002/2014WR016604

Temmerman, S., Bouma, T., Van de Koppel, J., Van der Wal, D., De Vries, M., & Herman, P. (2007). Vegetation causes channel erosion in a tidal landscape. *Geology*, *35*(7), 631–634. https://doi.org/10.1130/G23502A.1

Tetzlaff, D., Soulsby, C., Bacon, P. J., Youngson, A. F., Gibbins, C., & Malcolm, I. A. (2007). Connectivity between landscapes and riverscapes—A unifying theme in integrating hydrology and ecology in catchment science? *Hydrological Processes*, *21*(10), 1385–1389. https://doi.org/10.1002/hyp.6701

Umgiesser, G., Ferrarin, C., Cucco, A., De Pascalis, F., Bellafiore, D., Ghezzo, M., et al. (2014). Comparative hydrodynamics of 10 Mediterranean lagoons by means of numerical modeling. *Journal of Geophysical Research: Oceans*, *119*, 2212–2226. https://doi.org/10.1002/2013JC009512

USGS. (2016). *U.S. Geological Survey (USGS) water data for the nation*. Retrieved from http://waterdata.usgs.gov/nwis/

Vandenbruwaene, W., Temmerman, S., Bouma, T. J., Klaassen, P. C., de Vries, M. B., Callaghan, D. P., et al. (2011). Flow interaction with dynamic vegetation patches: Implications for biogeomorphic evolution of a tidal landscape. *Journal of Geophysical Research*, *116*, F01008. https://doi.org/10.1029/2010JF001788

Viero, D. P., & Defina, A. (2016). Water age, exposure time, and local flushing time in semi-enclosed, tidal basins with negligible freshwater inflow. *Journal of Marine Systems*, *156*, 16–29. https://doi.org/10.1016/j.jmarsys.2015.11.006

Wagner, W., Lague, D., Mohrig, D., Passalacqua, P., Shaw, J., & Moffett, K. (2017). Elevation change and stability on a prograding delta. *Geophysical Research Letters*, *44*, 1786–1794. https://doi.org/10.1002/2016GL072070

Walker, N. D. (2001). Tropical storm and hurricane wind effects on water level, salinity, and sediment transport in the river-influenced Atchafalaya-Vermilion Bay System, Louisiana, USA. *Estuaries*, *24*(4), 498–508. https://doi.org/10.2307/1353252

Walker, N. D., & Hammack, A. B. (2000). Impacts of winter storms on circulation and sediment transport: Atchafalaya-Vermilion Bay Region, Louisiana, U.S.A. *Journal of Coastal Research*, *16*(4), 996–1010.

Wang, C.-F., Hsu, M.-H., & Kuo, A. Y. (2004). Residence time of the Danshuei River estuary, Taiwan. *Estuarine, Coastal and Shelf Science*, *60*(3), 381–393. https://doi.org/10.1016/j.ecss.2004.01.013

Werner, T., & Kadlec, R. (2000). Wetland residence time distribution modeling. *Ecological Engineering*, *15*, 77–90. https://doi.org/10.1016/S0925-8574(99)00036-1

Wilcock, P. R. (1996). Estimating local bed shear stress from velocity observations. *Water Resources Research*, *32*(11), 3361–3366. https://doi.org/10.1029/96WR02277

Wörman, A., & Kronnäs, V. (2005). Effect of pond shape and vegetation heterogeneity on flow and treatment performance of constructed wetlands. *Journal of Hydrology*, *301*(1–4), 123–138. https://doi.org/10.1016/j.jhydrol.2004.06.038

Yu, K., DeLaune, R., & Poeckx, P. (2006). Direct measurement of denitrification activity in a Gulf coast freshwater marsh receiving diverted Mississippi River water. *Chemosphere*, *65*, 2449–2455. https://doi.org/10.1016/j.chemosphere.2006.04.046

Yuan, D., Lin, B., & Falconer, R. (2007). A modelling study of residence time in a macro-tidal estuary. *Estuarine, Coastal and Shelf Science*, *71*(3–4), 401–411. https://doi.org/10.1016/j.ecss.2006.08.023

Zektser, I., & Loaiciga, H. A. (1993). Groundwater fluxes in the global hydrologic cycle: Past, present and future. *Journal of Hydrology*, *144*(1–4), 405–427. https://doi.org/10.1016/0022-1694(93)90182-9

Zimmerman, J. (1976). Mixing and flushing of tidal embayments in the western Dutch Wadden Sea part I: Distribution of salinity and calculation of mixing time scales. *Netherlands Journal of Sea Research*, *10*(2), 149–191. https://doi.org/10.1016/0077-7579(76)90013-2